Electronic Supplementary Material (ESI) for Green Chemistry.
This journal is © The Royal Society of Chemistry 2020

[Electronic Supplementary Information]

Early-Stage Evaluation of Emerging CO_2 Utilization Technologies at Low Technology Readiness Levels

Kosan Roh[a], André Bardow[b,c,d,e], Dominik Bongartz[a], Jannik Burre[a], Wonsuk Chung[f], Sarah Deutz[c], Dongho Han[f], Matthias Heßelmann[g], Yannik Kohlhaas[g], Andrea König[a], Jeehwan S. Lee[f], Raoul Meys[c], Simon Völker[c], Matthias Wessling[g,h], Jay H. Lee[*,f], Alexander Mitsos[*,b,a,d]

[a]Process Systems Engineering (AVT.SVT), RWTH Aachen University, Forckenbeckstraße 51, 52074 Aachen, Germany

[b]JARA-ENERGY, 52056 Aachen, Germany

[c]Institute of Technical Thermodynamics (LTT), RWTH Aachen University, Schinkelstraße 8, 52062 Aachen, Germany

[d]Institute of Energy and Climate Research - Energy Systems Engineering (IEK-10), Forschungszentrum Jülich GmbH, 52425 Jülich, Germany

[e]Department of Mechanical and Process Engineering, ETH Zurich, Tannenstrasse 3, 8092 Zürich, Switzerland

[f]Department of Chemical and Biomolecular Engineering, Korea Advanced Institute of Science and Technology (KAIST), 291 Daehak-ro, Yuseong-gu, Daejeon 34141, Republic of Korea

[g]Chemical Process Engineering (AVT.CVT), RWTH Aachen University, Forckenbeckstraße 51, 52074 Aachen, Germany

[h]DWI-Leibniz Institute for Interactive Materials, Forckenbeckstraße 50, 52074 Aachen, Germany

*Corresponding authors: jayhlee@kaist.ac.kr; amitsos@alum.mit.edu

1. Description of Low TRLs and Specification to CO_2 Utilization Technologies

Emerging CU technologies usually tend to fall within TRLs of 2, 3, and 4 considering their lab- and bench-scale development states. Each low TRL is described as follows:

TRL 2 At this level, 'Technology concept and/or application is formulated, and patent research is conducted[1]'. There is little to no proof of concept via experiments for the technology as it is an abstract idea. For CU, one can come up with CO_2 conversion reactions that are thermodynamically feasible (e.g., a change in Gibbs free energy less than a certain value [2]), electrochemically feasible reactions for CO_2 reduction, and biomass feedstock originating from CO_2, and, if desired, potential value-added products and associated reactions.

TRL 3 At this level, 'Applied laboratory research is started, functional principle/reaction (mechanism) is proven, and predicted reaction is observed (qualitatively)[1]'. The concept of the idea formulated at TRL 2 has to be proven via active experimental research at the bench scale. By conducting actual experiments, a range of feasible operating conditions such as temperature and pressure for converting CO_2 into value-added products are roughly decided. In addition, various catalysts for accelerating the rate of CO_2 conversion reactions and/or enhancing the selectivity toward desired products are identified, and relevant reaction mechanisms are also verified at this level [3]. For electrochemical CO_2 conversions, high current density is aimed for lowering capital costs. Similarly, for biological CO_2 conversion, productivity and yield of desired components should be as high as possible.

TRL 4 At this level, 'Concept is validated in laboratory environment, scale-up preparation is started, and conceptual process design is conducted (e.g., based on simulation with simple models)[1]'. The experimentally proven idea should be implemented at the system level. Further experiments and process models developed for processes at TRL 4 can be used for performance improvements by finding operating

conditions, catalysts, and equipment design that show better performance than at TRL 3. Thus, the range of feasible operating conditions verified at TRL 3 becomes narrower at this level. Using the experimental data, modeling, and simulation for conceptual process design can be conducted to generate additional data required for tasks such as mass and energy balances and equipment sizing.

TRL 2 corresponds to Class 5 (Concept screening) while TRL 3 and 4 fall into Class 4 (Study or feasibility) of the cost estimate classification published by Association for the Advancement of Cost Engineering (AACE) International [4].

If a system is comprised of multiple processing units with different TRLs, the TRL of the entire system corresponds to the lowest level among the units [5].

2. Detailed description of the Evaluation Procedure Proposed

2.1 TRL-Dependent Primary Data

At TRL 2, the concept of the idea is formulated mostly without doing experiments. Thus, the primary data available at TRL 2 are limited to the basic physical properties of chemical components and reactions. Various databases of experimental reactions and property data for pure components and mixtures have been established (see Table SI 1 in ESI 1). Missing properties of desired components can be estimated by several methods, such as the UNIFAC model [6], which can be used for estimating the activity coefficients of non-ideal liquid mixtures.

Experimental data available at TRL 3 usually involves CO_2 conversion reactions or biomass growth experiments as the transformation of CO_2 into value-added chemicals is of key interest in CU research. The range of feasible operating conditions for a target reaction is defined at this level. The performance of such

reactions in small scales can be characterized. The size of the experimental apparatus can also be considered if available. Alternatives for unit operations can be identified.

The type of the primary data available at TRL 4 is very similar to TRL 3, but they are scaled up and closer to the industrial operation. Through conducting new experiments with well-performing catalysts and/or bigger reactors with advanced design and operation strategy, the reaction performance becomes improved and the range of operating conditions is narrowed. Furthermore, the size of the actual experimental apparatus should be available and at scales much larger than those employed at TRL 3. Unit operations for the whole process should be detailed.

2.2 TRL-Independent Primary Data

Table SI 1. Examples of TRL-independent primary data and relevant sources

Category	Data specification	Example data source
Reaction and component	Chemical formula and molecular weight of components Reaction stoichiometry	
Market and business	Raw material price[a]	7–9
	CO_2 capture cost[b]	10–14
	Utility price	15
	Product price[c]	7–9
	Carbon emission credit price	16
	Available market demand	17–19
	Correlations for equipment purchasing cost estimation[d]	20–23
	Investment costs for water electrolyzer	24
Carbon emission factor	Carbon footprint for raw material acquisition	25–28
	Carbon footprint for utility acquisition[e]	5,27–29
	Carbon footprint for product consumption/disposal	27,28,30,31
	Carbon footprint of reference/benchmark production[e,f]	25,27,28
Energy	CO_2 capture energy[b]	14,32–34
	Energy demand for raw material acquisition	25
	Energy content of raw materials and products[e]	35

[a]Exclude CO_2 feedstock.
[b]Include compression and transport of captured CO_2 if required.
[c]May not be available at low TRLs if target products or their applications are brand new.
[d]Only if the equipment is manufactured by mature technologies.
[e]Include production and transport of raw material and utility.
[f]Include both the main product and byproducts to be sold.

2.3 Secondary Data Calculation Strategy

2.3.1 Calculation at TRL 2

Mass Balance: Stoichiometries of CO_2 conversion reactions are the essential primary data for calculating the mass balance of the reaction section. The minimum amount of raw material (including CO_2) consumption can be calculated under the assumption of no undesirable side reactions taking place. This also extends to biological conversion of CO_2 in which the minimum requirement is determined by the fixation rates determined by photosynthesis. It is convenient to calculate the mass balance if biomass is expressed as pseudo-components. For example, $C_{106}H_{263}O_{110}N_{16}P$ represents a chemical formula of algal biomass based on elemental fractions of the primary biomass components [36]. If byproducts are generated by main reactions, separation is required to purify the main product. At TRL 2, perfect separation (100% recovery and purity of products) can be assumed by default unless more detailed information is available.

Energy Demand: In the case of thermochemical CO_2 conversion, if CO_2 conversion reactions are endothermic, the heat of reaction at the standard conditions (298 K, 1 atm) is assumed to be the thermal energy demand. If conversion reactions are exothermic, the possibility of thermal heat recovery is excluded at TRL 2 since the reaction temperature is unknown and the quality of the recovered energy is not guaranteed. Similarly, for electrochemical CO_2 conversion, the minimum electric power for the reaction is equivalent to the Gibbs free energy change.

For biological CO_2 conversion, minimum solar energy required for microalgae growth can be calculated to 114 kcal of free energy per 1 mole of CO_2 fixed as glucose by photosynthesis[37]. The operation conditions are relatively mild, so the energy demands in places such as mixing and temperature control are excluded if they are not available.

Energy demand for product separation is excluded at TRL 2 as it tends to be less significant than the energy demands for (endothermic) CO_2 conversion reactions or acquisition of raw materials with high-energy content such as hydrogen. This strategy is acceptable as 100% reaction conversion is assumed so that generation of undesirable side-products is excluded. Hence, it is not necessary to separate unreacted components for recycle and side-products for product purification.

2.3.2 Calculation at TRL 3

Mass Balance: Actual experimental data, including reaction conversion, selectivity, Faradaic efficiency, yield, and productivity, are used to calculate mass balances of the reaction section. Herein, these experimental data are assumed to be independent of the equipment size. For the separation section, perfect separation is assumed for all the conversion cases unless actual experimental data is available. Suitable separation technologies and their sequences can be identified based on the physical, structural, and chemical properties of participating components using the methodology of Jaksland [38]. Unreacted components are recycled with a reasonable purge ratio. The reaction conversion and selectivity of desired reactions at TRL 3 are usually not at 100%. Therefore, in order to produce the same amount of a product, the predicted raw material consumption is higher at TRL 3 than at TRL 2.

Energy Demand: For thermochemical CO_2 conversion, the heat of reaction at feasible operating conditions can be calculated by verified experimental data for deriving thermal energy demand. For electrochemical CO_2 conversion, electric power can be calculated by referring to the actual voltage applied and current density measured. The calculated power is most likely higher than the ideal power obtained at TRL 2 due to energy lost via cell over-potential [39]. For biological CO_2 conversion, one can refer to experimental results directly for information on energy and heat duties at the bench scale, which can be used to extrapolate accordingly. Separation energy demand can be calculated on the basis of experimental results. If no experimental data is available, the minimum work of separation that considers only entropy

changes [40] could be calculated. However, this likely leads to underestimations (c.f. the evaluation results of Case Study 2). If a conversion reaction proceeds at high pressure and in the vapor phase, it is highly recommended to calculate work for compressing feed streams.

Equipment Size: The first step in estimating the equipment size is to specify a target production capacity of CO_2 utilization (CU) processes. Then, the size of the actual experimental apparatus can be used to estimate the equipment size necessary to ensure the target production capacity. At TRL 3, we recommend estimating the size of major equipment such as reactors, compressors, and distillation columns that are prone to account for the largest portion of the total capital investment. Also, we assume that the process performances (e.g., reaction conversion, selectivity, and separation energy demand), which are measured or given in literature are independent of the scale of equipment. Another way is to use the aforementioned process simulators to estimate the equipment size such as the diameter and height of distillation columns and tanks; the area of heat exchangers; and the capacity of compressors, pumps and turbines (only if their power demands are computed).

2.3.3 Calculation at TRL 4

Mass Balance: As with TRL 3, one can refer to experimental data for information such as reaction conversion, productivity, and selectivity (or Faradaic efficiency for the electrochemical conversion and yield for the biological conversion) to calculate the mass balances. Alternatively, shortcut models with reaction conversion, productivity, and selectivity as inputs can be utilized to establish an overall mass balance (e.g., the Droop model for microalgae growth rate calculation [41]). Experimental data can also be referred to for the separation part. If experimental data is missing but thermodynamic model parameters are given, process simulations with rigorous separation models can be performed to design separation processes. Otherwise, perfect separation with 100% recovery must be assumed. Unreacted components can

be recycled with a reasonable purge ratio. If separation or purge generates off-gas that is combustible, off-gas combustion with air to recover thermal energy should be considered.

Energy Demand: In the reaction section, the enthalpies of reaction are updated based on more realistic operation conditions provided at TRL 4. In addition, the energy demand for temperature and pressure change in the process streams should be calculated. Simple heat exchanger networks can be synthesized via pinch analysis [42–44]. Energy demand for the separation by distillation/absorption/extraction columns can be estimated by rigorous process simulation or short-cut methods such as the Rectification Body Method (RBM) with sharp-split separation assumption embedded in EE-Toolbox [45–53].

Equipment Size: The analysis strategy to estimate the size of equipment at TRL 4 is almost the same as that at TRL 3. However, the size of the experimental apparatus at TRL 4 is generally bigger than that at TRL 3. If experiments are performed by using an apparatus with different sizes, a correlation between the equipment size and the process performance, such as reaction conversion, selectivity, and productivity, can be established. This correlation can be used to estimate the accurate size of the equipment, which is required for achieving the target production capacity. Moreover, we recommend estimating the size of minor equipment such as heat exchangers, pumps, etc. in addition to the major equipment.

2.4 Performance Indicator Calculation

Material Material-related indicators indicate how efficient CU technologies utilize the carbon source supplied. In particular, carbon efficiency plays a key role in biomass processing since higher reaction conversion and selectivity are of interest. Without complicated analysis, mass balances are only necessary for calculating the indicator. The way of calculating the material indicators is the same for all the low TRLs,

Energy Energy-related indicators indicate how efficient CU technologies consume the supplied energy to produce desired products. Because CO_2 is a very stable molecule, significant amounts of energy

are required for its transformation. Therefore, energy indicators are an intuitive method for evaluating the technology performance at a glance. The way of calculating the energy indicators is the same for all the low TRLs, but more elements for the net energy input are considered at higher TRLs. The amount of energy consumed for raw material acquisition, including CO_2 capture, and the amount of energy contained in raw materials (e.g., natural gas) can be added to the process energy input if these values do not significantly change with respect to the TRL.

Energy efficiency is a useful indicator when the final product of CU technologies can be consumed as fuel. The heating value of the product mainly accounts for the net energy output. For non-fuel products, specific energy consumption is a more appropriate indicator. It is advisable to convert different types of energy into primary energy by considering the conversion factors [54]. Some example factors are given in. Sometimes, calculating exergy instead of energy leads to more accurate evaluation results as exergy takes into account the quality of energy [55].

Table SI 2. Primary energy conversion factors for various utilities [54]

Energy inputs	**Primary energy conversion factors**
Natural gas	1.02–1.25
Naphtha	1.08–1.24
Electricity (generic, Europe)	2.49–2.93
Electricity from photovoltaics	1.00–1.25
Steam	1.13

GHG reduction Specific GHG reduction is an indicator that shows whether a CU technology can reduce GHG emissions throughout its life cycle. In other words, the carbon footprint of a CU process must be lower than that of its alternative or benchmark cases. The indicators can be calculated by conducting LCA. Specific GHG reduction should be positive if net GHG reduction is to be pursued. Since the GHG reduction potential accounts for the market demand of CU products, CU products with a big market demand are advantageous as they can replace larger quantities of fossil-based products [56].

There are guidelines for the calculation of GHG reduction indicators regarding suitable system boundaries [5,57,58]. For a CU process producing an equal (final) product as the corresponding alternative, the use phase (downstream) is identical. Thus, so-called cradle-to-gate system boundaries could be defined. If final products of a CU process differ from its alternative but their applications are equal, the entire life cycle has to be included, i.e., use and end-of-life and cradle-to-grave system boundaries are recommended [59]. For instance, conventional gasoline and diesel can be replaced by CO_2-based methanol [60] and CO_2-based OME [61], respectively. Moreover, CU processes often provide more than one product, i.e., a multi-functional system that has to be taken into account [5]. The problem of multi-functionality is not CCU-specific and can be found (or is comprehensively discussed) in the LCA methodology [62]. In addition, inventory data for construction and deconstruction of a plant with immature technologies are hardly available. Before the actual implementation, referring to GHG emission data of similar cases, e.g., conventional processes consisting of similar equipment, helps to roughly estimate the data.

Economics Economics-related indicators are used for evaluating the economic viability of CU technologies. These indicators are motivated by Buchner et al. [63]. Cost is classified as either operating costs, which are related to the operation of a business, or capital costs (commonly known as total capital investment), which include initial investment costs for equipment purchasing, delivery and installation, and working capital. Raw material, energy, and utility purchasing costs can be easily calculated once their unit prices, mass balances, and energy demand are given; direct operating costs (DOC) can be calculated at all the TRLs. At TRL 3 and 4, the capital cost can be estimated if the size of equipment is known and the equipment is manufactured by mature technologies [64]. In this case, it is recommended to calculate a 1-year depreciation (or annualized capital) cost by considering the equipment lifetime and interest rate. A comprehensive review about capital investment estimation for early-stage evaluation of chemical and biochemical processes can be found in Tsagkari et al. [65]. Indirect operating costs (IOC) such as maintenance costs, overhead, and laboratory costs can be calculated at TRL 3 and 4 if reliable data are available. At low

TRLs, costs for waste disposal and flaring are not considered unless these costs are expected to be significantly high.

For major process equipment based on new technologies, estimating their purchasing costs at larger scales is often difficult. For instance, most of the electrolyzers for CO_2 reduction show very low current densities. Compensating the low current densities by increasing the number of utilized electrolyzers increases the capital costs and thus significantly reduces the profitability [66]. One option is to exclude capital costd by considering only operating costs. Another option is to conduct a sensitivity analysis by perturbing the capital cost. If the economics-related indicators are sensitive to the capital cost, a goal can be set that guarantees economic competitiveness in the market.

If the market price of the final product already exists, gross operating margin (GOM) or specific profit can be calculated by subtracting all the cost terms from expected revenue. Additional revenue from carbon emission credits can also be included. For new products with nascent markets, calculating only the DOC or cost of goods manufactured (COGS) is a good approach. These costs can then be compared with existing alternatives to assess their competitiveness in the market.

When a CU technology is retrofitted to an existing process, it may either increase or decrease overall GOM or specific profit while preferably reducing GHG emissions. Such changes should be accounted for when evaluating the technologies.

Combined GHG reduction and economics When the GOM or specific profit obtained by a newly implemented CU technology is negative but the specific GHG reduction anticipated is positive, one can combine the economic and GHG reduction indicators to calculate the GHG avoidance cost (or the so-called cost of GHG or CO_2 avoided). This indicator represents the costs of avoiding one ton of CO_2 equivalent emitted. The costs for CO_2 compression, transport, and sequestration can serve as a benchmark for comparing the avoidance costs of CU technologies, as they both represent the price for avoiding GHG emissions. Additionally, the value of a GHG avoidance cost can be considered as being equal to the

minimum value of subsidies or carbon emission credits that fully compensate for the CU processes. If a CU technology is implemented to an existing process as a retrofit, one needs to calculate how much GOM or specific profit is newly obtained post-retrofit. Such a change can be both positive and negative. When the retrofit results in a net cost burden but a positive specific GHG reduction or difference of carbon footprint, a GHG avoidance cost can be calculated.

3. Databases, Methods, and Computer-aided Tools for Assisting the Evaluation Procedure

Table SI 3. Databases, methods, and computer-aided tools applicable for the CU technology analysis and evaluation

Task	Type	Name	Relevant literature	Website
Stoichiometry analysis	Database	Reaxys®		67
		SciFinder®		68
		DIPPR®801		69
		DDBST		70
		DETHERM		71
		NIST Chemistry WebBook		35
Process flowsheeting, simulation, and optimization	Tool	Aspen Plus®		72
		Aspen HYSYS®		73
		PRO/II®		74
		CHEMCAD		75
		SuperPro Designer®		76
		ProCAFD	77	78
		FSOpt	79	
Thermodynamic and physical property prediction	Tool	ProPred	80	81
		COSMOtherm	82,83	84
		Aspen Plus®		72
Minimum separation energy prediction	Tool	EE-Toolbox		45
	Method	RBM	46–53	
LCA	Tool	ecoinvent		25
		SimaPro		85
		GaBi		28
		LCSoft	86,87	88
		GEMIS		27
TEA	Tool	APEA		89
		ECON		90
		ESTEA		91
Combined LCA-TEA	Tool	ArKa-TAC^3	58	92
		TIPE-CCUS	93	
Monte Carlo simulation	Tool	@RISK		94
Optimization	Tool	GAMS		95
		FICO® Xpress		96
		Pyomo	97,98	
Network synthesis and analysis	Method	RNFA	99	
		PNFA	100	

4. Case Study 1: Electrochemical CO_2 Reduction for Value-Added Chemical Production

4.1 Primary Data

Table SI 4. Electrochemical reactions for producing ten value-added chemicals.

Product	Chemical reaction	Number of electrons (z)
Carbon monoxide	Cathode: $CO_2 + 2H^+ + 2e^- \rightarrow CO + H_2O$ Anode: $H_2O \rightarrow 2H^+ + 2e^- + 0.5O_2$ Overall: $CO_2 \rightarrow CO + 0.5O_2$	2
Formic acid	Cathode: $CO_2 + 2H^+ + 2e^- \rightarrow HCOOH$ Anode: $H_2O \rightarrow 2H^+ + 2e^- + 0.5O_2$ Overall: $CO_2 + H_2O \rightarrow HCOOH + 0.5O_2$	2
Formaldehyde	Cathode: $CO_2 + 4H^+ + 4e^- \rightarrow HCHO + H_2O$ Anode: $2H_2O \rightarrow 4H^+ + 4e^- + O_2$ Overall: $CO_2 + H_2O \rightarrow HCHO + O_2$	4
Methanol	Cathode: $CO_2 + 6H^+ + 6e^- \rightarrow CH_3OH + H_2O$ Anode: $3H_2O \rightarrow 6H^+ + 6e^- + 1.5O_2$ Overall: $CO_2 + 2H_2O \rightarrow CH_3OH + 1.5O_2$	6
Methane	Cathode: $CO_2 + 8H^+ + 8e^- \rightarrow CH_4 + 2H_2O$ Anode: $4H_2O \rightarrow 8H^+ + 8e^- + 2O_2$ Overall: $CO_2 + 2H_2O \rightarrow CH_4 + 2O_2$	8
Ethylene	Cathode: $2CO_2 + 12H^+ + 12e^- \rightarrow C_2H_4 + 4H_2O$ Anode: $6H_2O \rightarrow 12H^+ + 12e^- + 3O_2$ Overall: $2CO_2 + 2H_2O \rightarrow C_2H_4 + 3O_2$	12
Ethanol	Cathode: $2CO_2 + 12H^+ + 12e^- \rightarrow C_2H_5OH + 3H_2O$ Anode: $6H_2O \rightarrow 12H^+ + 12e^- + 3O_2$ Overall: $2CO_2 + 3H_2O \rightarrow C_2H_5OH + 3O_2$	12
Ethane	Cathode: $2CO_2 + 14H^+ + 14e^- \rightarrow C_2H_6 + 4H_2O$ Anode: $7H_2O \rightarrow 14H^+ + 14e^- + 3.5O_2$ Overall: $2CO_2 + 3H_2O \rightarrow C_2H_6 + 3.5O_2$	14
Propanol	Cathode: $3CO_2 + 18H^+ + 18e^- \rightarrow C_3H_7OH + 5H_2O$ Anode: $9H_2O \rightarrow 18H^+ + 18e^- + 4.5O_2$ Overall: $3CO_2 + 4H_2O \rightarrow C_3H_7OH + 4.5O_2$	18
Oxalic acid	Cathode: $2CO_2 + 2H^+ + 2e^- \rightarrow C_2H_2O_4$ Anode: $H_2O \rightarrow 2H^+ + 2e^- + 0.5O_2$ Overall: $2CO_2 + H_2O \rightarrow C_2O_4^{2-} + 0.5O_2$	4

Table SI 5. Primary data assumed for the evaluation of ten chemicals via electrochemical CO_2 reduction.

Specification	Value	Unit	Note	Ref.
Carbon footprint of product i		kg-CO_2eq/kg_i	Taken from open literature	
Methane	1.135		LNG imported from Australia to China, Shanghai	101
Oxalic acid	-0.822		Starch flour feedstock used	102,103
Price of raw material r		USD/kg_r		
Carbon dioxide	0.048		Representative CO_2 capture cost at a coal-fired power plant.	10
Process water	0.001		Deionized water	104
Price of product i		USD/kg_i		
Carbon monoxide	0.600			105
Formic acid	0.616			8
Formaldehyde	0.971			8
Methanol	0.437			106
Methane	0.522			107
Ethylene	1.084			108
Ethanol	0.525			109
Oxalic acid	0.650		Average price	110
Propanol	1.50			7
Ethane	0.194			7
Oxygen	0.05			111
Price of Renewable electricity	26.5	USD/GJ	Levelized cost of electricity (LCOE) of wind on-shore in South Korea, estimated for 2030 (5.5% discount factor)	112
Utility consumption for CO_2 capture				
LP steam	3.5	GJ/t-CO_2	Capture at a coal-fired power plant (13 mol.% CO_2)	33
Electricity	0.3	GJ/t-CO_2	Capture at a coal-fired power plant (13 mol.% CO_2)	33
Global market demand of product i		Mt-Prod/yr		
Carbon monoxide	3.60		Estimated for 2017	113
Formic acid	0.62		Estimated for 2012	114
Formaldehyde	23.1		Estimated for 2019	115
Methanol	97.1		Estimated for 2019	115
Methane	250		Unspecified	116
Ethylene	862		Estimated for 2016	117
Ethanol	546		Estimated for 2017	118
Oxalic acid	0.19		Estimated for 2009	119
Propanol	0.22		Sum of 1-Propanol (estimated for 2014) and n-Propanol (estimated for 2005)	120,121
Ethane	3.72		Estimated for 2018	

Table SI 6. LCA datasets for the evaluation of ten chemicals via electrochemical CO_2 reduction. Carbon footprints are taken from the LCA database ecoinvent 3.6 [122] and are evaluated with the Life Cycle Impact Assessment method Environmental Footprint 2.0 2018 midpoint.[123]

Process	**Dataset name**	**Region**	**Note**
Product			
Carbon monoxide	carbon monoxide production	GLO	For partial combustion of heavy fuel oil
Formic acid	formic acid production, methyl formate route	GLO	
Formaldehyde	oxidation of methanol	GLO	
Methanol	methanol production	GLO	For natural gas reforming
Ethylene	market for ethylene, average	RoW	Product out of steam cracking of naphtha
Ethanol	ethanol production from maize	GLO	
Propanol	1-propanol production	GLO	Synthesis from propanal
Ethane	ethane extraction, from natural gas liquids	GLO	
Oxygen	air separation, cryogenic	GLO	Mass-based impact allocation applied.
Electricity			
from wind turbine, onshore	electricity production, wind, 1-3MW turbine, onshore	KR	For the electrolyzer cell
from coal power plant	electricity production, hard coal	KR	For CO_2-capture at coal power plant
Heat	heat production, at hard coal industrial furnace 1-10MW	RoW	For CO_2-capture at coal power plant
Process water	market for water, deionized	RoW	

4.2 Evaluation Results

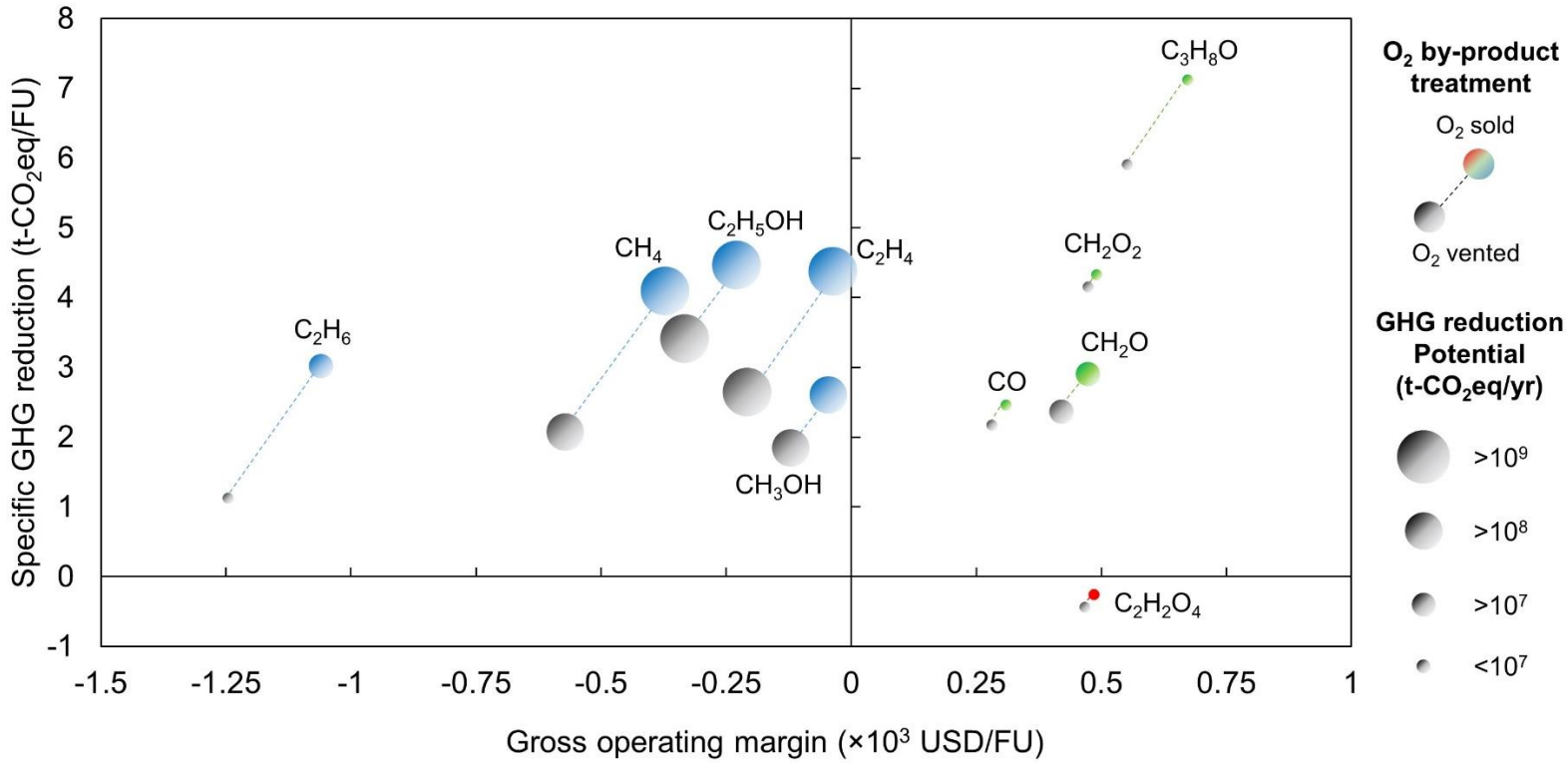

Figure SI 1. Evaluation results of ten electrochemical CO_2 conversion technologies on TRL 2 in the South Korean market. The functional unit is 1 ton of the target product and X ton of oxygen. The value of X depends on the target product. The size of the dots indicates the scale of their GHG reduction potential. Green: profitable and able to reduce GHG emissions. Red: profitable but unable to reduce GHG emissions. Blue: non-profitable but able to reduce GHG emissions. Dashed lines connect two dots that correspond to the two scenarios about how to treat oxygen byproduct. As more electrons are transferred during the reaction, more oxygen byproduct is produced, which results in the farther distance between the two dots.

5. Case Study 2: Electrochemical Ethylene Production via Co-electrolysis of CO_2 and H_2O

5.1 Detailed Technology Description

The reactions occur at an electro-catalytically active surface by applying an electrical potential. Recent studies focus on the increase of CO_2 reduction rate and long-term stability to enable fast commercialization of the technology [124–127]. De Arquer et al. [125], e.g., introduced a new catalyst preparation method that improves the partial current density for ethylene up to 13 kA/m^2 at 45% cathodic energy efficiency. Thus, electrochemical conversion of CO_2 might become a promising alternative to conventional ethylene production by steam cracking of hydrocarbons [128,129].

5.2 Primary Data

Table SI 7. Primary data assumed for the evaluation of electrochemical ethylene production.

Specification	Value	Unit	Note	Ref.
TRL-dependent parameter				
Faradaic efficiency of compound i		%	Minor side-products with below 2% of Faradaic efficiency are ignored	130
Ethylene	79.5			
Hydrogen	9.3			
Carbon monoxide	2.4			
Methane	5.8			
Voltage	2.4	V	42.8 % of exergy efficiency	130
Current density	46.1	mA/cm^2		130
Per-pass conversion of CO_2	24.3	%		130
TRL-independent parameter				
Price of raw material r		USD/kg_r		
Carbon dioxide	0.048		Representative CO_2 capture cost at a coal-fired power plant.	10
Process water	0.001		Deionized water	104
Monoethanolamine (MEA)	2.75		Make-up at CO_2 recovery unit	131
Price of product i		USD/kg_i		
Ethylene	1.084			108
Oxygen	0.05			111
Price of utility j		USD/GJ_j		
Renewable electricity	26.5		Levelized cost of electricity (LCOE) of wind on-shore in South Korea, estimated for 2030 (5.5% discount factor)	112
Grid electricity	21.9		For industrial use in South Korea	132
LP steam	12.8		Combustion (75% energy efficiency) of LNG	107
Cooling water	0.21		Taken from Aspen Plus®	
Equipment price				
Electrolyzer cell	1,080	USD/kW	Assume that cell configuration and materials are similar to chlor-alkali membrane electrolysis (1,000 EUR/kW)	133
Membrane	54	USD/m^2		134
Utility consumption for CO_2 capture				
LP steam	3.5	$GJ/t\text{-}CO_2$	Capture at a coal-fired power plant (13 mol.% CO_2)	33
Electricity	0.3	$GJ/t\text{-}CO_2$	Capture at a coal-fired power plant (13 mol.% CO_2)	33
Membrane permeance		GPU	Assume the membrane thickness of 70 nm	135
Carbon dioxide	732			

Ethylene	104		
Methane	28		
Carbon monoxide	12		
Hydrogen	80		
Miscellaneous			
Annual operating hour	8,000	hr	
Off-gas combustion efficiency	75	%	For heat recovery

Table SI 8. LCA datasets for the evaluation of electrochemical ethylene production. Carbon footprints are taken from the LCA database ecoinvent 3.6 [122] and are evaluated with the Life Cycle Impact Assessment method Environmental Footprint 2.0 2018 midpoint.[123]

Process	**Dataset name**	**Region**	**Note**
Product			
Ethylene	market for ethylene, average	RoW	Product out of steam cracking of naphtha
Oxygen	air separation, cryogenic	GLO	Mass-based impact allocation applied.
Electricity			
from wind turbine, onshore	electricity production, wind, 1-3MW turbine, onshore	KR	For the electrolyzer cell and product separation
from power grid	market for electricity, medium voltage	KR	For product separation
from coal power plant	electricity production, hard coal	KR	For CO_2-capture at coal power plant
Heat	heat production, at hard coal industrial furnace 1-10MW	RoW	For CO_2-capture at coal power plant
Process water	market for water, deionized	RoW	
Cooling water	market for water, decarbonized	RoW	For product separation
Mono-ethanolamine (MEA)	market for monoethanolamine	GLO	

Table SI 9. The primary data required for the evaluation of electrochemical ethylene production at TRL 2, 3 and 4.

Specification	Required data at TRL 2	Additionally required data at TRL 3	Additionally required data at TRL 4
Reaction and component	- Chemical formula, molecular weight, standard enthalpies of formation, standard entropies, and specific chemical exergy of reactant and product molecules - Reaction stoichiometry		
Experimental data		- Voltage - Current density - Faraday efficiency - Per-pass conversion of CO_2	
Market and business[a]	- Prices of raw materials[b], products, and renewable electricity	- Prices of industrial electricity and electrolyzer cell - TEA factors	- Price of membrane - Equipment cost correlations for the separation process - TEA factors
Carbon emission factor[a]	- Carbon footprints of raw materials[b], renewable electricity and product production (via conventional ways)	- Carbon footprint of power grid	- Carbon footprint of cooling water and MEA production
Miscellaneous			- Unit operations detailed and respective equipment - Gas permeation unit (GPU) of gas components - Vapor-liquid equilibrium data for simulation of product separation units - Combustion efficiency for heat recovery

[a] Available at all the TRLs.
[b] Captured CO_2 and deionized water.

5.3 Secondary Data Calculation

Mass Balance

At TRL 3 and 4, the mass balance of the co-electrolysis process for ethylene synthesis is calculated in Microsoft Excel using experimental data from Yano et al. [130]. Faraday's law is used to calculate the amount of each reaction product formed

$$\dot{n}_i = \frac{FE_i \, j_{geom} \, A_{geom}}{z_i \, F}$$

where $\dot{n}_i$ is the molar production rate of reactant i, FE_i is the faradaic efficiency taken from the experiments from Yano et al., z_i is the number of electrons transferred, F is the Faraday constant, and j_{geom} is the current normalized to the geometrical surface area of the electrode A_{geom}. The geometrical area of the electrode is calculated for a process capacity of 20 kt-C_2H_4/yr. The required amount of CO_2 $\dot{n}_{CO2,in}$ for the electrolysis is calculated using the conversion efficiency of the co-electrolysis:

$$\text{conversion} = \frac{\sum \dot{n}_i}{\dot{n}_{CO2,in}}$$

At TRL 4, the process flowsheet presented in Figure 5 is implemented in Aspen Plus® to calculate the mass balance for the downstream process. NRTL is chosen as the thermodynamic model for the membrane process, and the amine scrubber. The cryogenic distillation is modeled using the Peng-Robinson equation of state. The solution diffusion model describes mass transport in the membrane model [136], which was implemented in Aspen Custom Modeler® and loaded into Aspen Plus®. The absorber and the stripper of the amine scrubbing process are simulated using RadFrac rate-based columns. For the cryogenic distillation, we refer to the process model of an air separation unit given in Aspen Plus library, which assumes no heat loss, no pressure drops, and 100% tray efficiency. The whole process model does not include the recycling of CO_2 into the electrolysis. Thus, to calculate the actual amount of CO_2 that needs

to be supplied from the coal fire plant, the amount of CO_2 separated by the downstream is subtracted from $\dot{n}_{CO2,in}$. All waste streams, including purge streams of each recycle stream (1% of recycled stream), and outlet streams of the cryogenic distillation, despite the ethylene-rich stream, are burnt stoichiometrically.

Energy Demand

At TRL 3 and 4, to calculate the electric energy required for the electrochemical reaction, Faradaic efficiency (ε), Gibbs free energy change ($\Delta G°$), and transferred number of electrons per number of CO_2 molecules (z) have to be found out for all reactions occurring in the given cell. The electric energy can be calculated as below:

$$E_{elec} = \frac{1}{\eta_E} \sum_{i \in rxn} \frac{\Delta G_i \varepsilon_i}{z_i}$$

where η_E is the exergy efficiency of the given electrochemical cell.

At TRL 3, the minimum separation work can be calculated by using entropy of mixing, ΔS_{mix} and enthalpy of mixing, ΔH_{mix} as below:

$$W_{sep} = T\Delta S_{mix} - \Delta H_{mix}$$

where R is the gas constant, and T is temperature of the flow. Besides, entropy of mixing, ΔS_{mix} is calculated as below:

$$\Delta S_{mix} = nR\left(\sum_{i \in outlet} x_i \, ln \, x_i - \sum_{i \in inlet} x_i \, ln \, x_i \right)$$

where n is mole of the flow, and x_i means the mole fraction of component i in the flow.

At TRL 4, the energy demand for compressors, heat exchangers, rectification columns, turbines, and distillation columns is directly taken from Aspen Plus®. The cryogenic distillation of the product separation requires cooling at -99 °C and -135 °C. Cooling energy at such low temperatures is provided by

compression refrigeration systems. For the cooling demand $Q_{0,\mathrm{Cooler}}$, the input electricity $W_{\mathrm{el,Cooler}}$ can be calculated from the energy efficiency ratio $\mathrm{EER}_{\mathrm{Cooler}}$ of the compression refrigeration system:

$$W_{\mathrm{el,Cooler}} = \frac{Q_{0,\mathrm{Cooler}}}{\mathrm{EER}_{\mathrm{Cooler}}}$$

The energy efficiency ratio $\mathrm{EER}_{\mathrm{Cooler}}$ is estimated according to Strobridge[137] and ter Brake et al.[138] by the energy efficiency ratio of the ideal Carnot cycle $\mathrm{EER}_{\mathrm{Carnot}}$ and the exergy efficiency η_{Exergy} of current compression refrigeration systems:

$$\mathrm{EER}_{\mathrm{Cooler}} = \mathrm{EER}_{\mathrm{Carnot}} \cdot \eta_{\mathrm{Exergy}}$$

By utilizing both energy and entropy balance of a compression refrigeration system, we calculate the energy efficiency ratio $\mathrm{EER}_{\mathrm{Carnot}}$ of the ideal Carnot cycle from the ambient temperature T_{h} and the refrigeration temperature T_{l}:

$$\mathrm{EER}_{\mathrm{Carnot}} = \frac{1}{\frac{T_{\mathrm{h}}}{T_{\mathrm{l}}} - 1}$$

The electricity demands of the compression refrigeration system are shown in Table SI 10 for an ambient temperature of 300 K and both refrigeration temperatures.

Table SI 10. Electricity demands of the compression refrigeration system for cryogenic distillation (at the TRL 4 analysis). The ambient temperature is assumed 300 K.

Specification	**Symbol**	**Value**		**Unit**
Refrigeration temperature	T_{l}	-99	-135	°C
Cooling demand	$Q_{0,\mathrm{Cooler}}$	0.16	0.04	MJ/kg-C_2H_4
Exergy efficiency[137,138]	η_{Exergy}	20	18	%
Energy efficiency ratio				
of Carnot cycle	$\mathrm{EER}_{\mathrm{Carnot}}$	1.38	0.85	–
of compression refrigeration system	$\mathrm{EER}_{\mathrm{Cooler}}$	0.28	0.15	–
Electricity demand	$W_{\mathrm{el,Cooler}}$	0.56	0.25	MJ/kg-C_2H_4

For cooling demands at temperature levels between 60 °C and 150 °C, cooling water can be used. The total cooling demand $Q_{0,\text{Cooling water}}$ is 17.46 MJ/kg-C_2H_4. With a specific heat capacity of 4.18 kJ/(kg·K) and a water temperature increase of 5 K, the required amount of cooling water is 835 kg/kg-C_2H_4.

Equipment Sizing

The equipment sizing is done based on the mass and energy balances for an ethylene production plant with a capacity of 20 kt-C_2H_4/yr. The electrolyzer cell area can be calculated by using electric energy E_{elec} mentioned earlier, cell voltage V_{cell}, and current density J as below:

$$A_{cell} = \frac{E_{elec}}{V_{cell} \times J}$$

where V_{cell} is equal to the ideal voltage divided by the exergy efficiency η_E:

$$V_{cell} = \frac{V_{ideal}}{\eta_E}$$

Despite the co-electrolysis process, the dimensions of the equipment are taken from Aspen Plus®. Compressors, pumps, and turbines are sized corresponding to their shaft power. The sizing of inter-stage heat exchangers is not considered in this analysis as a rigorous network design is not yet available at this stage of development.

Table SI 11 to Table SI 14 summarize the secondary data calculated.

Table SI 11. Secondary data calculated and relevant costs for the electrochemical ethylene production at the TRL 3 and 4 analyses - Raw materials and utilities.

Specification	**Amount Consumed** TRL 3	TRL 4	**Unit**
Raw Material			
CO_2	71,989	75,289	t/yr
Utilities			
Electricity	2,504,142	2,837,771	GJ/yr

Cooling water	-	328,681	GJ/yr
Monoethanolamine	-	31	t/yr
Process water	37,553	108,499	t/yr

Table SI 12. Secondary data calculated and relevant costs for the electrochemical ethylene production at the TRL 3 analysis – Equipment.

Specification	**# of Units**	**Dimensions**	**Unit Cost**		**Equipment cost (MM USD)**	**Ref.**
Electrolyzer cells	29,019	A: 2.7 m^2	479	USD/t-C_2H_4	84.6	133
				Total	**84.6**	

Table SI 13. Secondary data calculated and relevant costs for the electrochemical ethylene production at the TRL 4 analysis – Equipment (H: Height, D: Diameter, V: Volume, S: Shaft power).

Equipment	**# of Units**	**Dimensions**	**Unit Cost**		**Equipment Cost (MM USD)**	**Ref.**
Electrolyzer cell	30,492	A: 2.7 m^2	503	USD/t-C_2H_4	98.38	133
				Subtotal	98.38	
Membrane process						
Membrane modules	2	A: 3,366 m^2 A: 846 m^2	1.16	USD/t-C_2H_4	0.23	134
				Subtotal	0.23	
Amine scrubber						
Absorber	1	H: 14.8 m D: 1.7 m	0.87	USD/t-C_2H_4	0.17	22
Stripper	1	H: 17.5 m D: 1.4 m	1.17	USD/t-C_2H_4	0.23	
				Subtotal	0.4	
Cryogenic distillation						
Distillation column	1	H: 28 m D: 0.6 m	1.05	USD/t-C_2H_4	0.21	22
				Subtotal	0.21	
Pumps & compressors						
Feed comp.	1	S: 2,067 kW	14.61	USD/t-C_2H_4	2.86	
Permeate comp.	1	S: 4,323 kW	38.23	USD/t-C_2H_4	7.48	
MEA pump	2	S: 2.2 kW S: 1.6 kW	0.06	USD/t-C_2H_4	0.01	22
Distillation comp.	1	S: 531 kW	6.17	USD/t-C_2H_4	1.21	
				Subtotal	11.55	
Turbines	2	S: 14.9 kW S: 25.7 kW	0.45	USD/t-C_2H_4	0.09	22

	Subtotal	0.09
	Total	**110.85**

Table SI 14. Secondary data calculated for the electrochemical ethylene production at the TRL 2 to 4 analysis – Functional unit basis.

Stream	Unit	TRL 2	TRL 3	TRL 4
Input				
CO_2	t/t-C_2H_4	3.14	3.60	3.74
Electricity	GJ/t-C_2H_4			
for electrolyzer cells		43.0	124.83	131.74
for separation process		-	0.37	9.94
for CO_2 capture		0.94	1.08	1.12
Heat for CO_2 capture		11.00	12.60	13.10
Refrigeration	GJ/t-C_2H_4			
at -99 °C		-	-	0.16
at -135 °C		-	-	0.04
Cooling water		-	-	
Energy basis	GJ/t-C_2H_4	-	-	16.48
Mass basis	t/t-C_2H_4	-	-	835.44
Monoethanolamine	t/t-C_2H_4	-	-	1.55E-3
Process water	t/t-C_2H_4	1.29	1.88	5.44
Output				
Ethylene	t/t-C_2H_4	1.00	1.00	1.00
Oxygen (emissions if not sold)	t/t-C_2H_4	3.43	4.18	4.41
Emission				
CO_2 from purge gas combustion	t/t-C_2H_4	-	0.46	0.61

5.4 Evaluation Results

Scenario Description

We define four scenarios:

S1: Renewable electricity is utilized at the whole ethylene plant; Oxygen byproduct is sold;

S2: Renewable electricity is utilized at the whole ethylene plant; Oxygen byproduct is vented;

S3: Renewable electricity is utilized for the electrolysis only while grid electricity is utilized for the product separation; Oxygen byproduct is sold;

S4: Renewable electricity is utilized for the electrolysis only while grid electricity is utilized for the product separation; Oxygen byproduct is vented.

Description of LCA study

The goal of this LCA is to compare the carbon footprint of two production processes for ethylene: (1) the CO_2-based electrochemical production of ethylene and (2) the fossil production of ethylene. The use phase and end-of-life phase of ethylene of both production processes are identical and thus cancel in a comparison. The system boundaries of the electrochemical ethylene production process combined with upstream CO_2 capture and downstream product separation are presented in Figure 4 of the manuscript. The technology is described in more detail in Section SI 5.1.

In LCA, a consistent comparison between two technologies requires using the same functional unit. [139] The electrochemical ethylene pathway is a multifunctional system that produces not only ethylene but also oxygen. To solve the multifunctionality problem, we consider a best-case and a worst-case scenario for the

oxygen byproduct. In the best-case scenario, we follow the approach presented by Jung et al. [62] and define oxygen as a valuable byproduct. Thus, we use the system expansion approach recommended by the ISO 14040/14044 norm [140,141] to solve multifunctionality problems in LCA: The fossil ethylene production system is expanded by oxygen production via cryogenic air separation to produce the same amount of oxygen as the electrochemical production process. Note that the coal power plant is a multifunctional system as well since it co-produces CO_2 besides electricity. We give a credit for CO_2 utilization according to von der Assen et al. [142] by applying the avoided burden approach. System expansion leads to the following functional unit in the best-case scenario: "production of 1 ton of ethylene and 4.41 ton of oxygen" for the TRL 4 analysis. However, utilization of the byproduct oxygen cannot always be guaranteed [143]. Therefore, in the worst-case scenario, we consider oxygen to be vented to air without any credit. Here, the functional unit is the "production of 1 ton of ethylene" for both the electrochemical and fossil ethylene production. In a sensitivity analysis, we subsequently assess the impact of electricity supply for downstream CO_2 recovery on the total carbon footprint of electrochemical ethylene production.

Mass and energy balances to generate the Life Cycle Inventory (LCI) are summarized in Table SI 14. The LCI collects all flows that are exchanged with the environment for a certain functional unit. Note that this study neglects the construction phases of the chemical plants due to a lack of data. The carbon footprints to supply the inputs for the electrochemical ethylene production are taken from the ecoinvent 3.6 database (Table SI 8). We chose datasets for South Korea, if available. Otherwise, we selected datasets for global or rest-of-the-world regions were as a proxy. For oxygen, the carbon footprint is estimated to be 0.51 kg-CO_2eq/kg-O_2 based on the electricity consumption for oxygen production and the carbon footprint of electricity from the Korean grid reported in the ecoinvent 3.6 database. We evaluate the carbon footprints using the *Climate Change, GWP 100a* [144] methodology, which is recommended by the Joint Research Center of the European Commission [123].

TEA results at TRL 4

For the cost analysis, capital cost and COGM are estimated based on cost models from Guthrie [22] and Turton et al. [20]. In this respect, carbon steel is considered as material for all units and a depreciation time of 10 years is assumed. Further details about the cost models can be found in Table SI 13 and Table SI 15.

The TEA considers two different scenarios (S1 & S2) for the electrochemical ethylene production. In the first scenario (S1), oxygen evolving in the anode reaction is sold as a byproduct of the electrolysis process. In the second scenario (S2), oxygen is released to the environment. However, in both cases, the specific profit is negative and -105 MM USD/yr for S1 and -109 MM USD/yr for S2. The negative profit is mainly attributed to the high energy consumption of the electrolysis process, which amounts to 53% of the COGM, see Figure SI 2. The equipment costs of the electrolysis amount to 19% and are the second largest contributor to the COGM. A decrease in equipment costs is expected when operating electrolyzers at industrial-relevant current densities greater than 200 mA/cm^2 [145]. However, operating at high current densities results in higher cell voltage. Thus, design optimization of the electrolysis is necessary to decrease the energy consumption of the process [124]. The downstream costs sum up to 6% of the COGM and are therefore small compared to the electrolysis process costs. If internal heat exchangers were considered, the investment costs of the downstreaming would increase.

Table SI 15. TEA results for the electrochemical ethylene production at the TRL 4 analysis: Production cost estimation for the ethylene process, with factors from Turton et al. [20]. S1 considers the sale of oxygen, while in S2, oxygen is vented into the air.

Total Equipment Cost (TEC)			**110,847,284**	**USD**
Raw material (C_{RM})			*3,613,890*	*USD/yr*
Waste treatment (C_{WT})			*0*	*USD/yr*
Utilities (C_{UT})			*75,543,133*	*USD/yr*
Operating labor (C_{OL})			687,700	*USD/yr*
Direct supervisory and clerical labor	*0.180*	* C_{OL}	123,786	*USD/yr*
Maintenance and repairs	*0.060*	* *TEC*	6,650,737	*USD/yr*
Operating supplies	*0.009*	* *TEC*	997,626	*USD/yr*
Laboratory charges	*0.150*	* C_{OL}	103,155	*USD/yr*
Patents and royalties	*0.030*	* *COM*	3,575,792	*USD/yr*
Total Direct Manufacturing Costs (DMC)	*Σ*		**91,295,918**	*USD/yr*
Depreciation	*0.100*	* *TEC*	11,084,728	*USD/yr*
Local taxes and insurance	*0.032*	* *TEC*	3,547,113	*USD/yr*
Plant overhead costs	*0.708*	* C_{OL}	486,892	*USD/yr*
	0.036	* *TEC*	3,990,502	*USD/yr*
Total Fixed Manufacturing Costs (FMC)	*Σ*		**19,109,235**	*USD/yr*
Administration costs	*0.177*	* C_{OL}	121,723	*USD/yr*
	0.009	* *TEC*	997,626	*USD/yr*
Construction and Installation	*0.110*	* *COM*	13,111,238	*USD/yr*
Contingency and Insurance	*0.050*	* *COM*	5,959,653	*USD/yr*
Total General Manufacturing Expenses (GE)	*Σ*		**20,190,240**	*USD/yr*
Cost of Goods Manufactured (COGM)	*DMC + FMC + GE*		**130,595,393**	*USD/yr*

		S1 (O_2 sold)	**S2 (O_2 vented)**	
Ethylene (main product)		21,624,889	21,624,889	*USD/yr*
Oxygen (byproduct)		4,395,612	0	*USD/yr*
Total Revenue (R)	*Σ*	26,020,502	21,624,889	*USD/yr*
Net Profit	*R - COGM*	**-104,574,892**	**-108,970,504**	*USD/yr*
Specific Profit		**-5.242**	**-5.462**	*USD/t-C_2H_4*

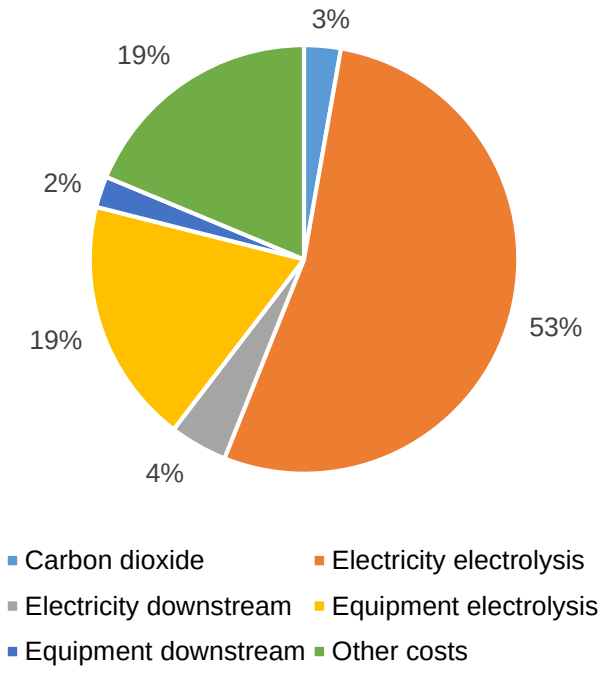

Figure SI 2. Distribution of the cost of goods manufactured for the electrochemical ethylene production (at the TRL 4 analysis).

LCA results at TRL 4

The cradle-to-gate carbon footprint of electrochemical ethylene production is compared to fossil ethylene production in Figure SI 3 for the worst-case scenario (S2). In this case, oxygen is considered an emission that is vented to air. Thus, the functional unit is "the production of 1 ton of ethylene". While the fossil ethylene production results in 1.53 t-CO_2eq/t-C_2H_4, electrochemical ethylene production yields a negative cradle-to-gate carbon footprint of -0.25 t-CO_2eq/t-C_2H_4. The carbon footprint is negative since CO_2 emissions otherwise emitted by the coal power plant to the atmosphere are avoided. The avoided emissions equal -3.74 t-CO_2eq/t-C_2H_4 (Figure SI 3). The heat from coal combustion for CO_2 capture at the coal power plant contributes most to the carbon footprint with 1.85 t-CO_2eq/t-C_2H_4. The next largest

contributions are caused by the electricity supply from onshore wind turbines for the electrolyzer cell and direct CO_2 emissions from purge gas combustion with approximately 0.61 t-CO_2eq/t-C_2H_4 each. In comparison to fossil ethylene production, the total carbon footprint can be reduced by 1.78 t-CO_2eq/t-C_2H_4, when ethylene is produced electrochemically.

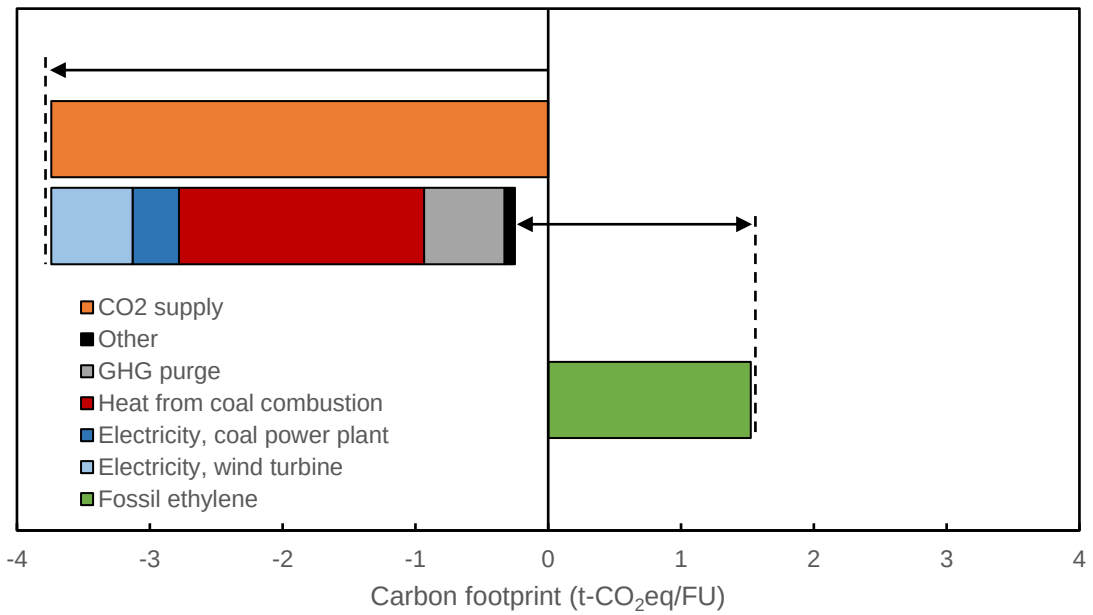

Figure SI 3. Cradle-to-gate carbon footprint of electrochemical ethylene production compared to fossil ethylene production (green) at the TRL 4 analysis. The functional unit is "the production of 1 ton of ethylene" because oxygen is considered an emission that is vented to air in the worst-case scenario (S2). CO_2 otherwise emitted by the coal power plant is negative (orange) while positive carbon footprints result from electricity production from onshore wind turbines (light blue) and a coal power plant (medium blue), heat from coal combustion at the coal power plant (red), direct CO_2 emissions due to purge gas combustion (grey) and minor CO_2 emissions from cooling water, process water, and monoethanolamine supply (black).

The cradle-to-gate carbon footprints for the best-case scenario (S1) are shown in Figure SI 4, where byproduct oxygen is considered a valuable product. In this case, the functional unit is "the production of

1 ton of ethylene and 4.41 ton of oxygen". Apart from oxygen production, all other contributions to the total carbon footprint are the same as in the worst-case scenario (S2) in Figure SI 3. Oxygen production via cryogenic air separation adds 2.23 t-CO_2eq to the carbon footprint of fossil production of 1 ton of ethylene and 4.41 ton of oxygen. As a result, the total carbon footprint of fossil production of ethylene and oxygen is now 3.75 t-CO_2eq per 1 ton of ethylene and 4.41 ton of oxygen. The increase of the carbon footprint of fossil production by considering oxygen a valuable product makes this the best-case scenario. As a result, electrochemical ethylene production can reduce the total carbon footprint by 4.00 t-CO_2eq per 1 ton of ethylene and 4.41 ton of oxygen.

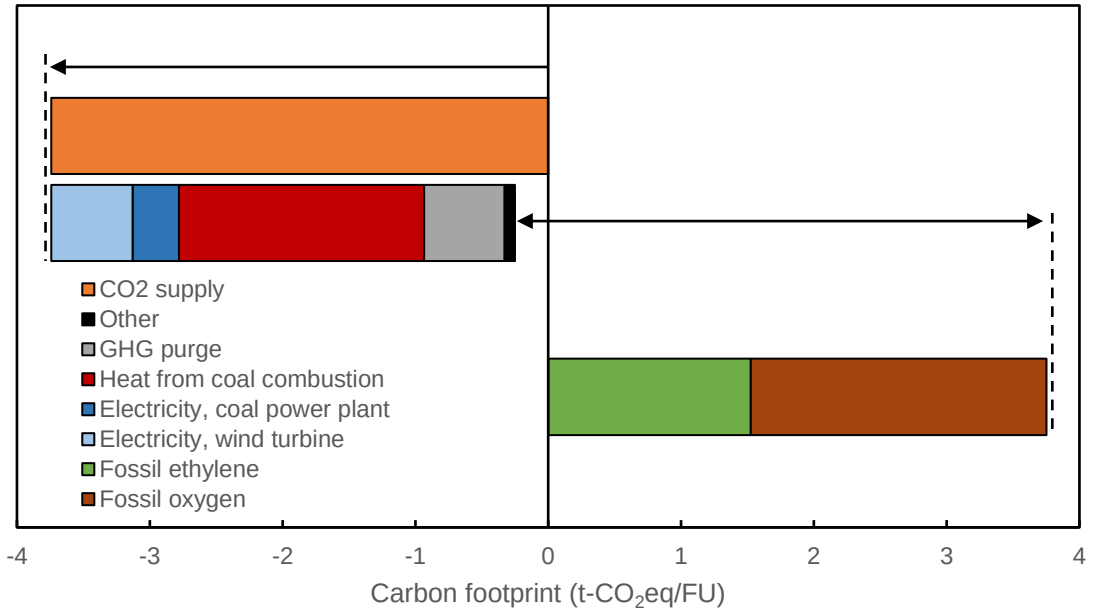

Figure SI 4. Cradle-to-gate carbon footprint of electrochemical ethylene and oxygen production compared to fossil production of ethylene (green) and oxygen (brown) at the TRL 4 analysis. The functional unit is "the production of 1 ton of ethylene and 4.41 ton of oxygen" because oxygen is considered a valuable product in the best-case scenario (S1). CO_2 otherwise emitted by the coal power plant is negative (orange). At the same time, positive carbon footprints result from electricity production from onshore wind turbines

(light blue) and a coal power plant (medium blue), heat from coal combustion at the coal power plant (red), direct CO_2 emissions due to purge gas combustion (grey) and minor CO_2 emissions from cooling water, process water, and monoethanolamine supply (black).

The cradle-to-gate carbon footprints for the sensitivity analysis of the worst-case (S4) and best-case scenario (S3) are shown in Figure SI 5 and Figure SI 6. For the sensitivity analysis, downstream CO_2 recovery and ethylene separation are supplied by electricity from the power grid instead of electricity from onshore wind turbines. Therefore, the contribution of electricity supply from onshore wind turbines reduces to 0.57 t-CO_2eq per functional unit in comparison to Figure SI 3 and Figure SI 4, while electricity supply from the power grid increases to 1.96 t-CO_2eq per functional unit. If electricity from the power grid is used for downstream CO_2 recovery and oxygen is vented to air (worst-case scenario, S4), electrochemical ethylene production results in 9% higher CO_2 emissions than fossil-based ethylene production (Figure SI 5). In the best-case scenario (S3, Figure SI 6), electrochemical ethylene production even reduces the total carbon footprint by 2.09 t-CO_2eq per functional unit compared to fossil-based ethylene and oxygen, if electricity for downstream CO_2 recovery and ethylene separation is supplied by the power grid.

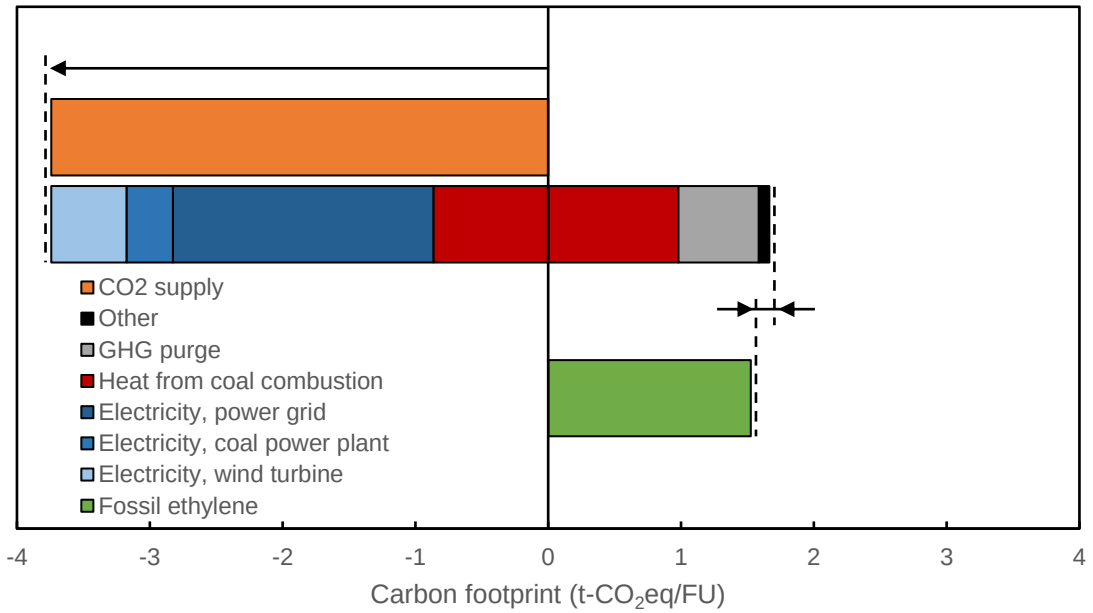

Figure SI 5. Sensitivity analysis for the cradle-to-gate carbon footprint of electrochemical ethylene production compared to fossil ethylene production (green) at the TRL 4 analysis. The functional unit is "the production of 1 ton of ethylene" because oxygen is considered an emission that is vented to air in the worst-case scenario (S4). CO_2 otherwise emitted by the coal power plant is negative (orange) while positive carbon footprints result from electricity production from onshore wind turbines (light blue), a coal power plant (medium blue) and the power grid (dark blue), heat from coal combustion at the coal power plant (red), direct CO_2 emissions due to purge gas combustion (grey) and minor CO_2 emissions from cooling water, process water, and monoethanolamine supply (black).

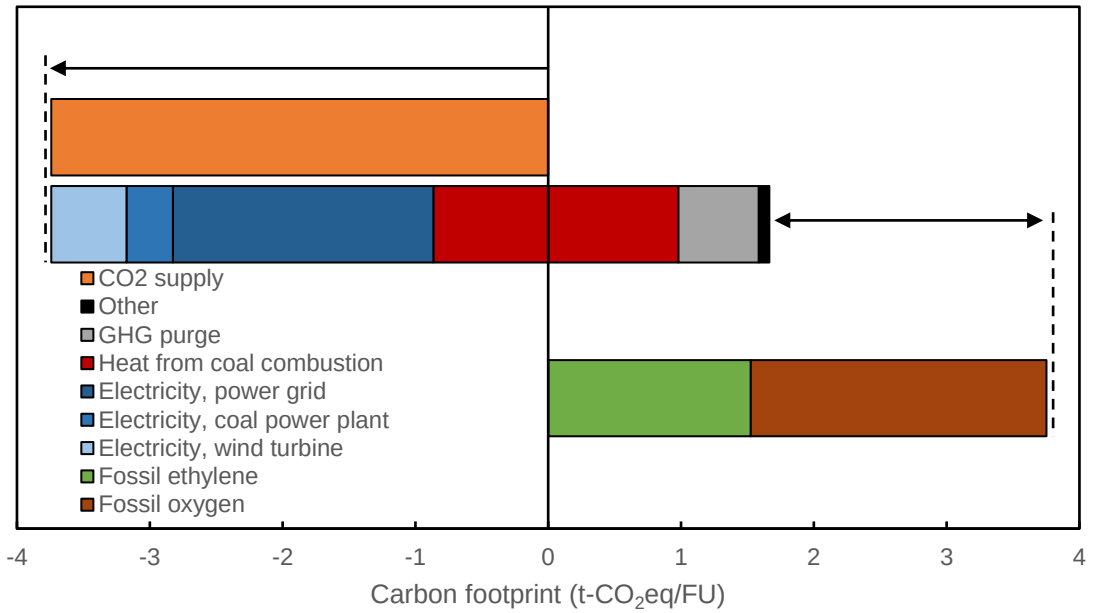

Figure SI 6. Sensitivity analysis for the cradle-to-gate carbon footprint of electrochemical ethylene and oxygen production compared to fossil production of ethylene (green) and oxygen (brown) at the TRL 4 analysis. The functional unit is "the production of 1 ton of ethylene and 4.41 ton of oxygen" because oxygen is considered a valuable product in the best-case scenario (S3). CO_2 otherwise emitted by the coal power plant is negative (orange) while positive carbon footprints result from electricity production from onshore wind turbines (light blue), a coal power plant (medium blue) and the power grid (dark blue), heat from coal combustion at the coal power plant (red), direct CO_2 emissions due to purge gas combustion (grey) and minor CO_2 emissions from cooling water, process water, and monoethanolamine supply (black).

6. Case Study 3: Thermochemical CO_2 Conversion for OME_1 Production via Direct Oxidation of Methanol (TRL 4)

6.1 Detailed Technology Description

The main reactions in the process are

$3H_2 + CO_2 \leftrightarrow MeOH + H_2O$, $\Delta H_r^{298K} = -49.3\ \mathrm{kJ/mol}$, (Eq. 1)

$3MeOH + 0.5O_2 \rightarrow OME_1 + 2H_2O$, $\Delta H_r^{298K} = -229.0\ \mathrm{kJ/mol}$. (Eq. 2)

Both are gas phase reactions that proceed over heterogeneous catalysts and are strongly exothermic. The first reaction is an equilibrium reaction, and elevated pressures (e.g., 70–80 bar) are required for good per-pass conversion (e.g., around 40%) at typical reaction temperatures in the range of 200–300 °C [146]. Catalysts can be either conventional catalysts used for methanol synthesis from syngas or special catalysts for CO_2 conversion [147]. The main side reaction to the first reaction is the reverse water gas shift reaction $H_2 + CO_2 \leftrightarrow CO + H_2O$. Formation of other side products (e.g., higher alcohols, esters, or hydrocarbons) is negligible [146]. For the second reaction, bifunctional catalysts have been developed that combine in-situ formation of formaldehyde and subsequent conversion to OME_1. Methanol conversions of up to 69% and selectivities of up to 99% have been reported at atmospheric pressure and at 100–300 °C in the presence of excess air. Depending on the catalyst, possible side products are formaldehyde, dimethyl ether, methyl formate, carbon monoxide, and CO_2 (e.g., [148–150]).

6.2 Primary Data

Table SI 16. Primary data assumed for the evaluation of the oxidative OME_1 production.

Specification	Symbol	Value	Unit	Note	Ref.
TRL-dependent parameter					
CO_2 raw material pressure	p_{CO2}	1	bar		
H_2 raw material pressure	p_{H2}	30	bar		
R1 reactor pressure	p_{R1}	70	bar		146
Gas hourly space velocity in R1	$GHSV_{R1}$	10,500	hr^{-1}		146
Molar educt ratio in R1	$r^{R1}_{H_2,CO_2}$	3			146
R2 reactor pressure	p_{R2}	1	bar		150
Gas hourly space velocity in R2	$GHSV_{R2}$	11,400	mL/(g.hr)		150
Methanol mole fraction in R2 inlet	$x_{R1,MeOH}$	5.3	mole %		150
Methanol conversion in R2		66	%		150
OME_1 selectivity in R2		93	%		150
TRL-independent parameter					
Low heating value of OME_1		23.4	MJ/kg		151
Plant capacity		200	kt/yr		
Annual operating hour		8,000	hr		
PEM electrolyzer electricity demand		55	kWh/kg-H_2		152
H_2 price		4,500	EUR/t-H_2	Produced by water electrolysis using wind power in Northern Germany in 2035	153
CO_2 price		0	EUR/t-CO_2	Available from an ethylene oxide plants in free	
Electricity price		0.134	EUR/kWh	The average price for industrial consumers in Germany with annual consumption between 20,000 and 70,000 MWh from 2007 to 2017 including all taxes	15

6.3 Secondary Data Calculation

Mass Balance

The process concept in Figure 6 is implemented in Aspen Plus® to solve the mass balance. The implemented flowsheet considers reactant recycling as well as off-gas combustion for energy recovery. NRTL [154] is chosen as the thermodynamic model. RPlug and RStoic models are used for the reactor R1 and R2, respectively. The gas-liquid separations are simulated using flash units. For the distillations, perfect separation is assumed, considering the known azeotrope between methanol and methylal, thus the separator models are used. To account for the latter, the distillation sequence for OME_1 purification is based on that presented by Weidert et al. [155] as the resulting mixtures are rather similar.

Energy Demand

The energy demand for compression, pumping, as well as heating and cooling in all units except distillation columns is taken directly from Aspen Plus®. The energy demand of the distillations is estimated using the Rectification Body Method (RBM) [46,51] available through our Energy Efficiency Toolbox [45]. The RBM calculates the pinch points for the rectification and stripping section of a distillation column; therefore, it estimates the minimum energy demand (i.e., that at minimum reflux ratio) while considering non-ideal thermodynamics of the mixtures using the NRTL model [154].

Additionally, a pinch analysis is conducted to investigate the potential for heat integration (minimum temperature difference of 5 K). To this end, the temperature-duty curves of all heat exchangers are examined and in case they are too nonlinear, the heat exchangers are divided into multiple parts such that each of the parts has an essentially linear temperature-duty curve. Since the gas-liquid separation after Reactor R2 requires very low temperatures to achieve good product recovery (e.g., -87 °C for less than 2% product loss), multiple cold utilities are assumed based on the grand composite curve, namely cooling water at 25°C, and low-temperature cooling at levels of -87 °C and -25 °C. The cost for the low-temperature cooling is estimated assuming an ideal refrigerating machine, i.e., providing the necessary exergy by electricity.

Equipment Sizing

Based on the energy and mass balances, an approximate sizing is conducted for major plant equipment such as distillation columns, reactors, compressors, and pumps. The potential market demand for OME_1 as fuel is comparable to the market of fossil diesel, as it can replace a significant amount of diesel. The total consumption of fossil diesel in Germany was almost 40 Mton in 2017 [156]. Thus, a large-scale production plant with a capacity of 200,000 t/yr is considered. Compressors and pumps are sized corresponding to their shaft power. The reactor sizes are determined by

$$V = \tau_{res}\dot{V}\epsilon$$

where τ_{res} is residence time (CO_2 hydrogenation: 10.8s; methanol oxidation: 0.3s), $\dot{V}$ volumetric flow rate (CO_2 hydrogenation: 2.7 m^3/s; methanol oxidation: 300 m^3/s), and ϵ bed voidage (CO_2 hydrogenation: 0.5). The height of distillation columns is based on the minimum reflux ratio given by the RBM, as well as the minimum number of trays given by the Fenske equation. Since a rigorous heat exchanger network is not yet available at this stage of development, heat exchanger sizing is omitted for now.

The secondary data of the process is summarized in Table SI 17 to Table SI 19.

Table SI 17. Secondary data calculated and relevant costs the evaluation of the oxidative OME_1 production – Equipment (H: Height, D: Diameter, V: Volume, S: Shaft power).

Equipment	**# of Units**	**Dimensions**	**Unit Cost**		**Equipment Cost (EUR)**	**Ref.**
Distillation columns						
Methanol purification	3	H: 13.8 m D: 2.8 m	0.221	EUR/t-OME_1	1,327,433	22
MF separation	2	H: 46.0 m D: 2.5 m	0.531	EUR /t-OME_1	2,123,894	
Methanol separation	3	H: 12.1 m D: 3.0 m	0.221	EUR/t-OME_1	1,327,433	

OME_1 purification	3	H: 42.6 m D: 2.7 m	0.664	EUR/t-OME_1	3,982,301	
				Subtotal	8,761,061	
Reactors						
Methanol reactor	1	V: 40.4 m³	0.044	EUR/t-OME_1	88,495	22
OME_1 reactor	1	V: 90.0 m³	0.102	EUR/t-OME_1	203,540	
				Subtotal	292,035	
Pumps & Compressors						
Azeotrope pump	1	S: 6.4 kW	0.009	EUR/t-OME_1	17,699	
H_2 comp.	1	S: 2,986.2 kW	1.062	EUR/t-OME_1	2,123,894	
CO_2 comp.	2	S: 2,355.8 kW	0.885	EUR/t-OME_1	3,539,823	22
Recycle 1 comp.	1	S: 1,046.4 kW	0.398	EUR/t-OME_1	796,460	
Recycle 2 comp.	1	S: 726.7 kW	0.310	EUR/t-OME_1	619,469	
				Subtotal	7,097,345	
				Total	**16,150,441**	

Table SI 18. Secondary data calculated and relevant costs for the evaluation of the oxidative OME_1 production - Raw materials and utilities.

	Amount Consumed		**Total Cost (EUR/yr)**
Raw Material			
H_2	51,080,000	t/yr	229,858,407
CO_2	371,680,000	t/yr	0
		Subtotal	229,858,407
Utilities			
Electricity for cooling at -23 °C	78,800	GJ/yr	2,932,743
Electricity for cooling at -23 °C	55,000	GJ/yr	2,045,133
Electricity for pumping and compression	273,000	GJ/yr	10,157,522
		Subtotal	15,135,398
		Total	**244,993,805**

Table SI 19. Secondary data calculated for the evaluation of the oxidative OME_1 production – Raw materials and utilities, functional unit basis.

Stream	**Unit**	**Value**

Input			
	H_2	kg/GJ-OME_1	10.96
	CO_2	kg/GJ-OME_1	79.88
	Electricity	MJ/GJ-OME_1	58.68
	Cooling water (25 °C)	MJ/GJ-OME_1	360.82
	Refrigeration (-23 °C)	MJ/GJ-OME_1	88.56
	Refrigeration (-87 °C)	MJ/GJ-OME_1	19.65
Output			
	OME_1	kg/GJ-OME_1	42.74
	CO_2 (in off-gas)	kg/GJ-OME_1	2.62
	MF	kg/GJ-OME_1	1.72
	H_2O	kg/GJ-OME_1	53.29

6.4 Evaluation Results

For the cost analysis, capital cost and COGM are estimated based on cost models from Guthrie [22] and Turton et al. [20]. In this respect, carbon steel is considered as material for all units, and a depreciation time of 10 years is assumed. A Chemical Plant Cost Index (CEPCI) of 567.5 from the year 2017 has been used [157]. Further details about the cost models can be found in Table SI 17 and Table SI 20.

Table SI 20. TEA results for the oxidative OME_1 production: Production cost estimation for the OME_1 process, with factors from Turton et al. [20].

Total Equipment Cost (TEC)			**16,150,441**	**EUR**
Raw material (C_{RM})			229,858,407	*EUR/yr*
Waste treatment (C_{WT})			*0*	*EUR/yr*
Utilities (C_{UT})			15,135,398	*EUR/yr*
Operating labor (C_{OL})			619,469	*EUR/yr*
Direct supervisory and clerical labor	*0.180*	* C_{OL}	111,504	*EUR/yr*
Maintenance and repairs	*0.060*	* *TEC*	969,026	*EUR/yr*
Operating supplies	*0.009*	* *TEC*	145,354	*EUR/yr*
Laboratory charges	*0.150*	* C_{OL}	92,920	*EUR/yr*
Patents and royalties	*0.030*	* *COM*	9,226,715	*EUR/yr*
Total Direct Manufacturing Costs (DMC)	*Σ*		**256,158,793**	**EUR/yr**
Depreciation	*0.100*	* *TEC*	1,615,044	*EUR/yr*
Local taxes and insurance	*0.032*	* *TEC*	516,814	*EUR/yr*
Plant overhead costs	*0.708*	* C_{OL}	438,584	*EUR/yr*
	0.036	* *TEC*	581,416	*EUR/yr*
Total Fixed Manufacturing Costs (FMC)	*Σ*		**3,151,858**	**EUR/yr**
Administration costs	*0.177*	* C_{OL}	109,646	*EUR/yr*
	0.009	* *TEC*	145,354	
Construction and Installation	*0.110*	* *COM*	33,831,287	*EUR/yr*
Contingency and Insurance	*0.050*	* *COM*	15,377,858	*EUR/yr*
Total General Manufacturing Expenses (GE)	*Σ*		**49,464,145**	**EUR/yr**
Cost of Goods Manufactured (COGM)	*DMC + FMC + GE*		**308,774,796**	**EUR/yr**

The COGM for the oxidative OME_1 production process is 66 EUR/GJ-OME_1, which is about twice the price of fossil diesel available in Germany in October 2018 including all taxes (i.e., 37 EUR/GJ-Diesel). As shown in Figure SI 7, the major cost drivers are the raw materials that account for 95% of the total production cost. Electricity costs for cooling at -87 °C and -25 °C make up about 1.6% of the total production cost. Additional electricity costs for pumping and compression make up about 3% of the total production cost. As mentioned above, no external heat needs to be provided to the process. Investment costs

are less than 1% of the total production cost. Distillation columns and compressors account for 54% and 44% of the investment cost, respectively. However, it should be noted that the heat exchangers are not included in the investment cost estimate since a heat exchanger network design is not yet available. In addition, catalyst costs are excluded due to the data not being available. Hence, the actual investment cost might be significantly higher.

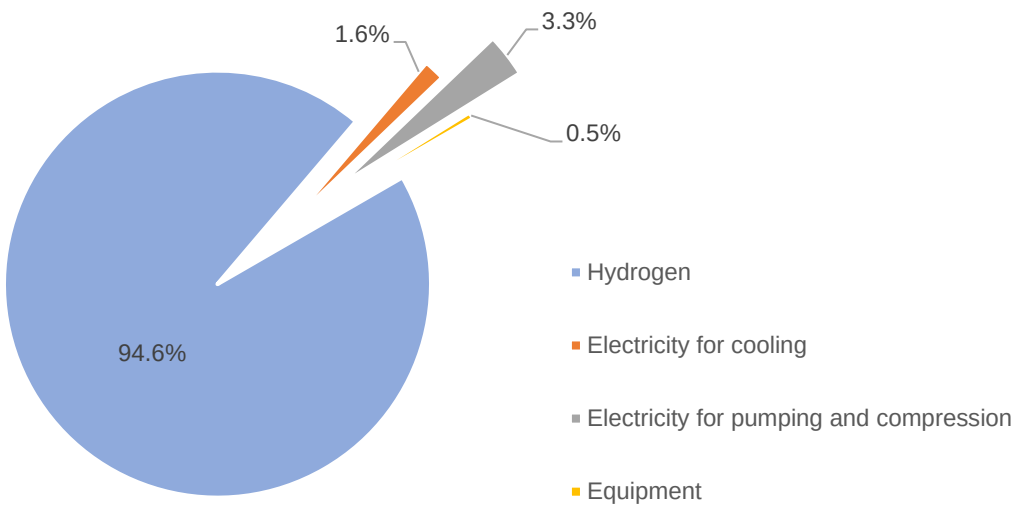

Figure SI 7. Distribution of the total production cost for the oxidative OME_1 production.

The required mass and energy balances for the Life Cycle Inventory phase that enter and leave the life cycle of OME_1 are taken from Table SI 21. The construction of the plant except the electrolyzer is neglected due to the lack of data at the early stage of development, and generally, it has a low influence on the GHG emissions compared to operation [158]. Lower bounds are considered for the supply of H_2, CO_2 and utilities, and a sensitivity study is conducted. The GHG emissions of all considered supply chains (cf. Table SI 21) are taken from the LCA database GaBi thinkstep AG [28] and are assessed based on the Life Cycle Impact Assessment method Environmental Footprint 2.0 2018 midpoint [123]. For the supply of H_2, a PEM-electrolyzer is considered as a baseline case. The LCI data for the PEM-electrolyzer is based on Bareiß et

al. [152] for the near future and the renewable scenario with 3,000 full load hours. We assume metal recycling corresponding to current global recycling rates based on Reuter et al. [159].

For the electricity supply, we consider wind power from the European Union, country-specific grid mixes today and global forecasts for 2030 and 2050. The global forecasted electricity grid mixes in 2030 and 2050 are based on the predicted shares of electricity generation in the beyond 2°C scenario of the Energy Technology Perspectives by the IEA [160]. For the electricity generation technologies, we assume German LCI datasets, since only country-specific LCI datasets are available. The generation of electricity by ocean and others (in 2030 < 0.07 % and in 2050 < 1.29 %) is neglected through missing LCI datasets and the small share. Furthermore, the beyond 2°C scenario comprises electricity generation technologies (coal, gas, and biomass) with carbon capture and storage (CCS). LCI datasets for CCS technologies are not available and are, therefore, modeled as conventional generation technologies, but the remaining GHG emissions are reduced according to the IPPC WGIII AR5 report [29].

Table SI 21. LCA datasets for the evaluation of the oxidative OME_1 production [28]. The LCI of the PEM-electrolyzer is based on Bareiß et al. [152] for the near future and the renewable scenario with 3,000 full load hours. Current global metal recycling rates are based on Reuters et al.[159]. The LCI of the electricity for Global is based on IEA report [161].

Process	Dataset name	Recycling rate	Region	Comment
Electrolyzer				
Activated carbon	*Activated carbon ts*		*DE*	
Aluminum	*Aluminum sheet mix ts*	*0.9*	*DE*	
Copper	*Copper mix (99,999% from electrolysis) ts*	*0.7*	*DE*	
Electronic material	*Electronic component production, passive, unspecified ts*		*GLO*	*Power, control*
Iridium	*Platinum mix ts*	*0.25*	*GLO*	*Iridium is a transition metal of the platinum group*
Low alloyed steel	*Steel plate ts*	*0.85*	*EU*	
Nafion	*Polytetrafluoroethylene granulate (PTFE) mix ts*		*DE*	*Sulfonated tetrafluoro-ethylene based fluoropolymer-copolymer*
Plastic	*Polyethylene production, high density, granulate ts*		*DE*	
Platinum	*Platinum mix ts*	*0.65*	*GLO*	
Process material	*Lubricants at refinery ts*		*DE*	*Adsorbent, lubricant*
Stainless steel	*Stainless Steel slab (X6CrNi17) ts*	*0.85*	*DE*	
Titanium	*Titanium ts*	*0.91*	*GLO*	
Electricity				
Belgium	*Electricity grid mix ts*		*BE*	
Canada	*Electricity grid mix ts*		*CA*	
Finland	*Electricity grid mix ts*		*FI*	
France	*Electricity grid mix ts*		*FR*	

Global 2030/2050	*Electricity from biomass (solid) & Electricity from waste ts (50:50)* *Electricity from geothermal** *Electricity from hard coal* *Electricity from hydro power* *Electricity from natural gas* *Electricity from wind power* *Electricity from photovoltaic* *Electricity from heavy fuel oil* *Electricity from nuclear*	*DE* **IS*	*Forecasting electricity grid mix under the beyond 2 ºC*
Iceland	*Electricity grid mix ts*	*IS*	
New Zeeland	*Electricity grid mix ts*	*NZ*	
Norway	*Electricity grid mix ts*	*NO*	
Sweden	*Electricity grid mix ts*	*SE*	
Switzerland	*Electricity grid mix ts*	*CH*	
Wind	*Electricity from wind power ts*	*DE*	
Diesel	*Diesel mix at filling station ts*	*DE*	
Hydrogen	*Hydrogen (steam reforming from natural gas) ts*	*DE*	

Figure SI 8 shows the carbon footprint from cradle-to-gate of the oxidative OME_1 production for the nominal case compared to fossil diesel. The resulting carbon footprint of the OME_1 production is negative. Negative emissions occur due to the CO_2 supply that assumes avoided emissions at the ethylene oxide plant. Negative cradle-to-gate emissions are required over the entire life cycle to reach carbon neutrality since the CO_2 emissions are subsequently released from gate-to-grave; namely during fuel combustion. The highest carbon footprint is caused by H_2 supply (electricity demand of the PEM electrolyzer) followed by the direct emissions and the electricity supply to run the process. Compared to the fossil diesel production, the GHG emissions could be reduced by 71.7 kg-CO_2eq/GJ-diesel by the oxidative OME_1 production.

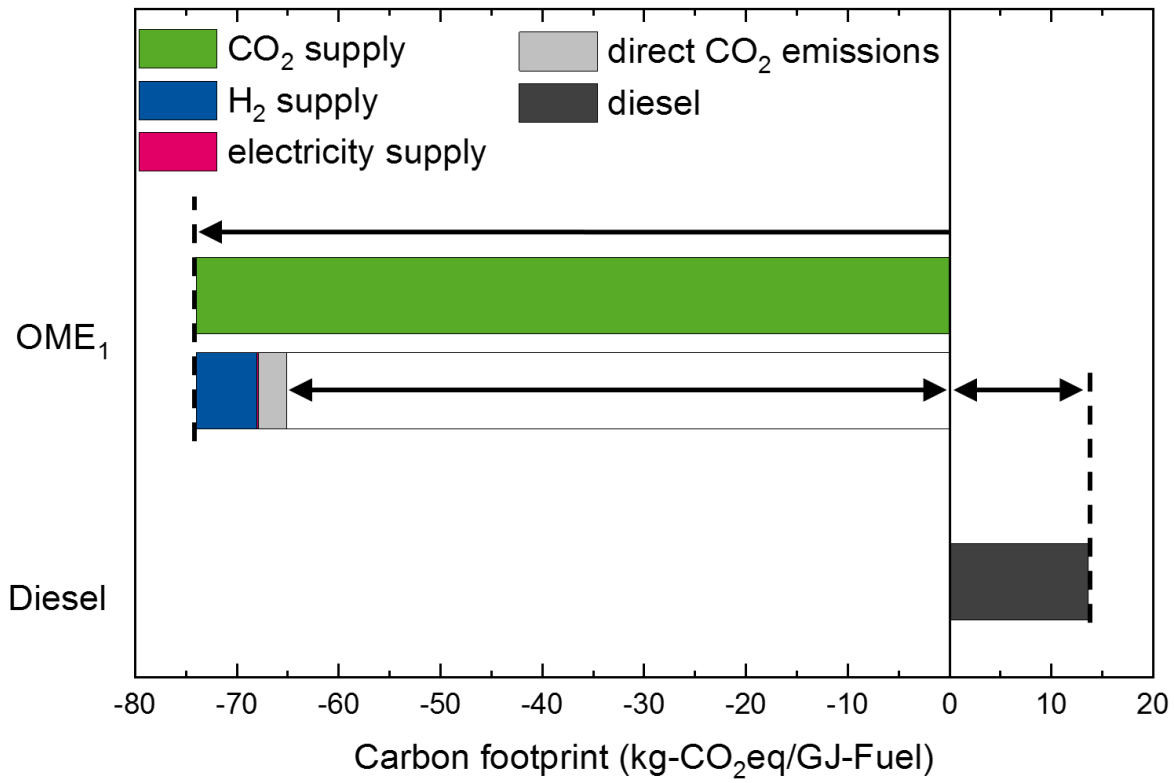

Figure SI 8. The carbon footprint for the oxidative OME_1 production for the nominal-case (-65.1 kg-CO_2eq/GJ-OME_1) compared to the fossil production (13.6 kg/GJ-diesel, average value for Germany [28]) from cradle-to-gate. The green bar represents the negative GHG emissions of CO_2 supply via an ethylene oxide synthesis and thus avoiding CO_2 emissions directly at the point source. The light grey, red and blue bars show the positive carbon footprint from the OME_1 production. The electricity supply includes the compression of H_2 from 30 bar to 70 bar and CO_2 from 1 bar to 70 bar. The dark grey bar represents the carbon footprint of the fossil diesel supply. The black arrows represent the resulting carbon footprint for the OME_1 production and the resulting reduction of GHG emissions via the substitution of fossil diesel.

7. Case Study 4: Biological CO_2 Conversion for Microalgal Biomass Co-Firing (TRL 4)

7.1 Detailed Technology Description

The core technology of the microalgal co-firing process is cultivation, where CO_2 is bio-fixed into algal cell biomass. The conversion of biomass for the production of value-added products usually involves either the (1) extraction and purification of native algal compounds (e.g., carotenoids, omega-3-fatty acids, etc.) or (2) depolymerization/pyrolysis/firing of entire biomass (e.g., biocrude, bio-gas, etc.). The former is often associated with metabolic engineering, while the latter tends to be more aligned with conventional fuel production technology. In microalgal biomass co-firing, the algal biomass grown in cultivation reactors are separated, dried, pelletized, and then fed directly into the coal-fired boiler to create a closed-loop CO_2 cycle. In addition, CO_2 that is not utilized by the algal cells can still remain dissolved in the cultivation broth as inorganic forms (HCO_3^-, CO_3^{2-}, CO_2) in which they are functionally sequestered from the environment.

At the process systems level, the rate of CO_2-to-biomass conversion is primarily mass transfer limited. These limitations occur at: (1) the gas/liquid interface for CO_2 supply (e.g., bubblers) to the cultivation media and (2) the algal cell wall (active transport of inorganic forms of CO_2) [162–164]. The enzymatic biofixation via *RuBisCO* post-active transport is energy-limited [165]. Currently, proposed models vary in detail and coverage of the above phenomena, especially at differing scales. The process engineering adopted in this work primarily concerns the mass transfer of CO_2 into the cultivation broth for modeling the rate of biomass formation at the systems level. For the cultivation reactors, modular and low-cost vertical airlift column photobioreactors with flue gas bubbling are considered. While pond reactors might be more economical on a volumetric basis, the large amount of land needed for pond reactors makes it impractical as the algal cultivation farm must be constructed within the vicinity of the coal power plant. In addition, the carbon utilization efficiencies of open pond reactors are significantly lower due to being an open system.

Consequently, further scaling-up is required to achieve the same amount of closed-loop sequestration as that in a photobioreactor. Recent advances in algal cultivation technology report feasible algal cultivation at less than 80 USD/m^3 [166]. For the cultivating species, *Chlorella vulgaris* was selected due to its high productivity and moderately high LHV. Fertilizers such as potassium sulfate and sodium nitrate are used to supplement nutrients required for cultivation.

The plant is operated as a fed-batch. Algal biomass is cultivated during the day and is harvested every two days. Daylight irradiation is assumed to be available for 12 hrs from 6 AM to 6 PM with an average specific growth rate of 1.07 hr^{-1} [34]. Cultivation nutrients are fed at the beginning of each day at the start of the batch cycle and resupplied at the 7th hour. The harvested broth at the end of every second day are pumped into a holding tank for concentration via electroflocculation. Electroflocculation uses charged electrodes which supply ions that induce the congregation of algae, resulting in floc formation. The broth is subsequently routed to a mixer-settler tank where the flocs accelerate the settling of algae [167], after which solid-liquid separation removes the microalgal biomass from the bulk media. The resulting algal slurry undergoes belt filtration in which water is removed continuously and in multiple stages via a vacuum suction. Water is removed in a final drying step in a convective dryer. Low temperature flue gas from the boiler stack (120–130ºC)[32] is routed to the belt dryer, and the waste heat is utilized to reduce the moisture content to below 10% [168]. Since the cultivation plant is well integrated with the CO_2 source plant, no heat loss is assumed during the flue gas transport.

In each biomass concentration process, the culture media containing water, nutrients, and residual biomass is collected, filtered, and recycled. Since no additional chemicals or bio-flocculants are added during the downstream processes, the filtered microalgae can be batch-added to the cultivation media to serve as inoculum. A small fraction of the recycled water is purged (blowdown) from the process to prevent the buildup of ions and recalcitrant organic material.

7.2 Primary Data

Table SI 22. Primary data assumed for the evaluation of the Microalgal Co-firing Plant.

Specification	Symbol	Value		Ref.
Land Requirement for Cultivation	$A_{cult.}$	83.48	ha	
pH	ph	9.5		[169]
Relative Flue Gas Flowrate	V_{fg}	0.07	vvm	
Plant Operating Hours	η_{opr}	8,322	hr	[170]
Cultivation Time per Harvest	$\Theta_{cult.}$	48	hr	[171]
Conversion yield of Carbon	Y_x	1211	10^9 cells	[172]
Volume per vertical bubble column	v_{col}	9.6	L/unit	[172]
Volumetric mass transfer coefficient	kLa	1.4	hr^{-1}	[172]
Half saturation constant for carbon	K_S	$4.7 \cdot 10^{-3}$	mmol/L	[173]
CO_2 dissociation constant	K_{CO2}	$10^{-6.35}$	mol/L	[172]
Bicarbonate dissociation constant	K_{Bic}	$10^{-10.3}$	mol/L	[172]
Partial Pressure of CO_2	P_{CO2}	0.136	Atm	[172]
Culture flowrate	f_{cult}	0.12	L/hr/unit	[172]
Exit Concentration, Electroflocculation	$\gamma_{\text{biomass}}^{\text{Har}}$	2	wt. %	[174]
Biomass Recovery, Electroflocculation	$\psi_{\text{biomass},1}^{\text{Har}}$	94.52	%	[175]
Exit Concentration, Vacuum Belt Filter	$\gamma_{\text{biomass}}^{\text{Dew}}$	25	wt. %	[176]
Biomass Recovery, Vacuum Belt Filter	$\psi_{\text{biomass},1}^{\text{Dew}}$	87.50	%	[176]
Exit Concentration, FG Drying	$\gamma_{\text{biomass}}^{\text{Dry}}$	90	wt. %	[168]
Biomass Recovery, FG Drying	$\psi_{\text{biomass},1}^{\text{Dry}}$	100	%	[168]

7.3 Secondary Data Calculation

Mass Balance

Because microalgae shares similarities with other microorganisms such as bacteria, classical bioprocess models can be incorporated for modeling the kinetics of biomass growth [172]. Specifically, Monod kinetics consider the concentration of external limiting nutrients in modeling the growth rate of algal cells [173]. In

comparison to models such as the Droop model, which considers internal nutrient storage, the Monod form offers two main advantages. First, the concentrations of external nutrients can be easily measured via experimental apparatus. Second, because the continuously resupplying media in the current process provide an excess of nitrates, phosphates, sulfates, and other trace metals, the Monod form can be simplified to only consider CO_2 as the limiting nutrient. The final form with Monod kinetics is as follows:

$$\mu = \mu_{max} \cdot \frac{[TIC]}{K_S + [TIC]} \quad \text{(Eq. 3)}$$

$[TIC]$ is the average concentration of total inorganic carbon and is calculated by taking the sum of the concentrations of CO_2, HCO_3^- and CO_3^{2-} in media. The concentrations of the latter two species are determined by the dissociation constants listed in Table SI 17 and the culture pH. Thus, CO_2 and TIC can be linked via the following equation:

$$[CO_2] = \frac{[TIC]}{1 + \frac{K_{CO_2}}{[H+]} + \frac{K_{CO_2} K_{Bic}}{[H+]^2}} \quad \text{(Eq. 4)}$$

The change in $[TIC]$ is represented by the following equation [172], which effectively models the mass transfer limitations aforementioned in Section 6.1:

$$\frac{d[TIC]}{dt} = -\frac{\mu X}{Y_x} + k_L a([CO_2^e] - [CO_2]) \quad \text{(Eq. 5)}$$

Equation 5 primarily concerns the CO_2 mass transfer from flue gas feed into media (macroscopic scale). The mass transfer limitation of CO_2 uptake by the cell walls are simplified with parameter Y_x, which represents the conversion yield of carbon species into biomass. $[CO_2^e]$ is the concentration of CO_2 that is in equilibrium with the overhead vapor phase and can be calculated using Henry's law:

$$[CO_2^e] = \frac{P_{CO_2}}{H} \quad \text{(Eq. 6)}$$

where P_{CO2} is the partial pressure of CO_2, which is determined by the feed rate and composition of incoming flue gas, and H is the Henry's law constant, which is 29.41 at mL/mol. Finally, the change in the concentration of algal cells in culture is modeled as a linear function of the current cell concentration times the specific growth rate, minus cells that are in circulation from the culture cycling:

$$\frac{dX}{dt} = \mu X - \frac{F}{V} X \qquad \text{(Eq. 7)}$$

where X is the concentration of cells in culture and has units 10^9 cells/L. Simultaneously solving for Eq. 3–6 given batch harvest time gives the amount of biomass produced per cycle as well as the rate of CO_2 consumption at each time step.

Monod kinetics with accompanying Equations 6–8 can sufficiently model the growth of *Chlorella vulgaris* cells in closed airlift bubble columns, as validated by Tebbani et al. [172]. However, the remainder of the mass balance concerning water and nutrient update (especially major, non-carbon nutrients such as N, P, S) must still be addressed. Unlike the previous case studies, biological conversion of CO_2 via microalgal cultivation involves numerous metabolic pathways in a way that an elementary/stoichiometric calculation of mass balances is often difficult. To address this issue, a component balance model can be constructed in which the basic mass units are compounds rather than chemical elements. This approach allows us to overcome difficulties in representing the synthesis/breakdown of complex organic material while still maintaining the semblance of an overall mass balance. A component mass balance for a component *i* for a reaction with no accumulation can be expressed as

$$F_i^{out} = F_i^{in} - R_K F_K^{in}(1 + R_{NK}) + \omega_P\left[\sum_K\left(R_K F_K^{in}\right) + \sum_{NK}\left(R_{NK} \cdot \sum_K\left(R_K F_K^{in}\right)\right)\right],$$

where F_i^{in} and F_i^{out} denote the total mass flow of component *i* entering and exiting a certain process unit, respectively. R_K is the fractional conversion of the key reacting component *K*. For microalgal cultivation, CO_2 is usually limiting, and as such, R_{CO_2} can be calculated experimentally by deriving the average

utilization rate with respect to the mass of CO_2 bubbled. R_{NK} is the reacted mass of non-key reacting components with respect to the key reacting component. Equation 8 shows an example of a component reaction for microalgal cultivation adopted from Dunlop and Coaldrake [177] with Table SI 17 displaying R_{NK} for each of the non-key reactants. Components that are generated from a reaction are represented by fractional component mass yields of a produced component P (ω_P), which is multiplied to the total reacted mass term. Note that, since multiple types of fertilizer salts are available, the component reaction for cultivation can be expressed in many different ways. Equation 8 is a simplified form of the formation reaction as unhindered microalgal growth requires numerous secondary nutrients such as magnesium, calcium, iron, zinc, etc., all of which are currently excluded from the overall balance [178].

$$46.29\ \mathrm{CO_2} + 3.84\ \mathrm{NO_3^-} + 0.079\ \mathrm{SO_4^{2-}} + 0.093\ \mathrm{HPO_4^{2-}} + 46.02\ \mathrm{H_2O} \rightarrow 1\ \mathrm{Microalgae} + 64.05\ \mathrm{O_2} + 4.17\ \mathrm{OH^-} \quad \text{(Eq. 8)}$$

Table SI 23. Specific consumption of major nutrients R_{NK} during cultivation as a function of CO_2 consumed.

Material	**Specific consumption during cultivation R_{NK} (kg/kg-CO_2 reacted)**
NO_3^-(representing nitrogen consumption)	0.1168
SO_4^{2-}(representing sulfur consumption)	0.0044
HPO_4^{2-}(representing phosphate consumption)	0.0039
H_2O	0.4070

Equipment Sizing and Energy Demand

The component balances establish a scale of flows from which equipment sizes and energy/utility consumptions can be calculated. These values are reported as either being specific to a particular reference flow or being specific to the capacity of a quoted equipment. Therefore, each unit process needs to be

investigated individually, and judgment on the analysis methods should be based on the type of primary data that is available. In the case where information is provided in terms of reference flows, appropriate scaling methods should be applied to calculate secondary data. Linear scaling is often used as the most basic form of estimation, but it can also result in severe over/under-estimations if the scales differ by several orders of magnitude. Utility consumptions for cultivation and electroflocculation processes are calculated by linearly scaling large-scale pilot plant data. In the latter, Lee et al. [167] report that electrode charging, hydraulic mixing, and settling for a large-scale electroflocculation module consumes up to 0.33 MJ/m^3 [167]. For the harvest of an 83 ha cultivation farm producing 1,335 tons-dry biomass/batch, this translates into an energy requirement of 88 GJ/batch. On the other hand, conventional process equipment such as pumps and heat exchangers can make use of widely available models or empirical relationships.

All the secondary data for the microalgal cultivation plant are given in Table SI 24 and Table SI 25.

Table SI 24. Secondary data calculated and cost parameter assumed for the evaluation of the Microalgal Co-firing Plant: Equipment sizing and purchasing cost.

Specification	# of Units	Unit Cost		Equipment Cost (USD)	Ref.
Vertical Airlift Column PBR					
Structural Forms		130.41	USD/t-algae	29,610,233	
Metal Fabrication		26.08	USD/t-algae	5,922,047	
Pond Airlift Piping, and Control		62.60	USD/t-algae	14,212,912	33
Gas Blowers		45.07	USD/t-algae	10,233,297	
Water Supply Equipment		190.57	USD/t-algae	43,270,248	
Plastic Tubing		21.30	USD/t-algae	4,835,921	
			Subtotal	108,084,658	
Electroflocculation					
Electrode Modules	33	660,000	USD/module	21,780,000	
Hydraulic Mixers	80	122,400	USD/mixer	9,792,000	167
Settlers and Tanks	33	523,475	USD/tank	12,424,256	
			Subtotal	43,996,256	
Vacuum Belt Filtration					
Belt, Filter and Motor	43	520,000	USD/unit	22,360,000	21
			Subtotal	22,360,000	
Convective Dryers					
Dryer, 1st Stage	20	300,000	USD/unit	6,000,000	21
Dryer, 2nd Stage	7	300,000	USD/unit	2,100,000	
			Subtotal	8,100,000	
Miscellaneous Major Equipment					
Centrifugal Pumps	5			234,437	
Gas Blowers	2			3,165,158	
Mixers	2			287,358	
Blowdown SLS	1			1,590,850	72,179
Grinder	1			153,573	
Other	N/A			58,900	
			Subtotal	5,490,276	
			Total	**188,031,190**	

Table SI 25. Secondary data calculated and cost parameter assumed for the evaluation of the Microalgal Co-firing Plant: Mass balances, energy demand, and relevant costs.

	Amount Consumed		**Total Cost (USD/yr)**
Raw Material			
N Fertilizer	46,966	t	16,692,281
P+S Fertilizer	2,044	t	408,452
CO_2 (from co-fired glue gas)	1,004,213	t	0 (Assumed)
Process Water	9,572	kt	1,435,734
		Subtotal	18,536,466
Utilities			
Blowdown Treatment	8,993	kt	3,489,484
Electricity On-site	513,447	GJ	13,970,906
		Subtotal	17,460,390
Credits			
Avoided Coal Feed	112,925	t	(4,865,923)
		Subtotal	(4,865,923)
		Total	**40,069,954**

7.4 Evaluation Results

The capital cost for the microalgal plant is estimated by adopting Lang Factors from Tredici et al. [180], which performed TEA of a 1 ha Green Wall Panel PBR for microalgal cultivation. Capital and operating costs for the coal plant are calculated using the EIA handbook for utility-scale electricity generating plants [181]. The study assumes a 30-year plant lifetime with a 3-year construction and a static interest rate of 8%. Based on these assumptions, the calculated depreciation factor is 0.089. The estimated capital investment is given in Table SI 26. GHG emissions incurred during the plant construction and salvage process are excluded from the system boundary for calculating the carbon footprint. The functional unit is 1 GJ of co-fired electricity generated.

Table SI 26. Capital investment estimated for the Microalgal Co-firing Plant, factors from Tredici et al. [180].

Total Equipment Cost (TEC)			**188,031,190**	**USD**
Equipment Installation (EI)	0.10	* TEC	18,803,119	USD
Total Installed Equipment Cost (TIEC)	TEC + Σ		**206,834,309**	**USD**
Piping, Fitting, Valves and Tanks	0.28	* TIEC	57,913,607	USD
Instrumentation, Controls, Electrical	0.54	* TIEC	111,690,527	USD
Field Laboratory	0.10	* TIEC	20,683,431	USD
Σ	0.92	* TIEC	190,287,565	USD
Total Direct Cost, (TDC)	TIEC + Σ		**190,287,565**	**USD**
Engineering and Supervision	0.05	* TDC	9,514,378	USD
Contingency	0.10	* TDC	19,028,756	USD
Insurance	0.01	* TDC	1,902,876	USD
Total Indirect Cost, (TIC)			**30,446,010**	**USD**
Fixed Capital Investment (Algal Plant)	TDC + TIC		**220,733,575**	**USD**
Fixed Capital Investment (Coal Plant)			**1,799,835,380**	**USD**
Working Capital Investment	0.05	* FCI	101,028,448	USD
Total Capital Investment	*FCI + TCI*		**2,121,597,403**	**USD**

A breakdown of the levelized cost of electricity (LCOE) and carbon footprint is shown in Figure SI 9 and Table SI 27, respectively.

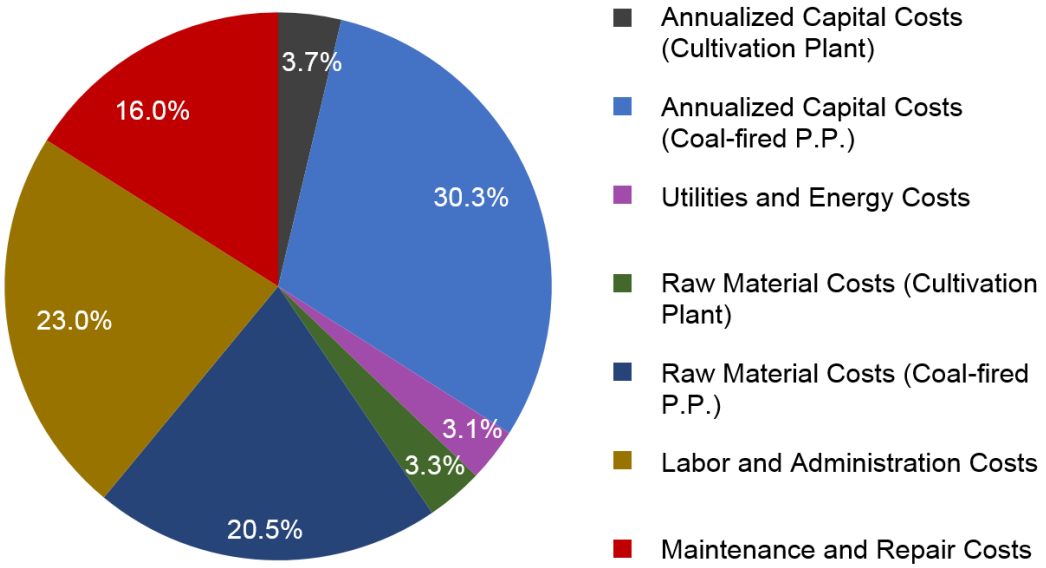

Figure SI 9. Breakdown of the LCOE for the microalgae co-fired plant.

Table SI 27. Summary of Emission Factors and GHG emissions for the Microalgal Co-firing Plant.

Specification	Emission factor		GHG emissions	
Direct Emission				
Boiler FG CO_2 to Stack	1.00	t-CO_2eq/t	0.117	t-CO_2eq/GJ_e
Vent CO_2 from Cultivator	1.00	t-CO_2eq/t	0.033	t-CO_2eq/GJ_e
		Subtotal	0.151	t-CO_2eq/GJ_e
Indirect Emission				
Coal (Mining & Supply)	0.32	t-CO_2eq/t	1.974E-2	t-CO_2eq/GJ_e
N-Fertilizers (Production)	4.62	t-CO_2eq/t	1.317E-3	t-CO_2eq/GJ_e
P/S-Fertilizers (Production)	2.70	t-CO_2eq/t	3.438E-4	t-CO_2eq/GJ_e
Electricity (Production)	0.13	t-CO_2eq/GJ	3.957E-3	t-CO_2eq/GJ_e
Water (Supply)	0.00	t-CO_2eq/t	0.000	t-CO_2eq/GJ_e
Wastewater Treatment	1.93E-3	t-CO_2eq/t	1.053E-3	t-CO_2eq/GJ_e
		Subtotal	3.826E-2	t-CO_2eq/GJ_e
		Total	**0.190**	**t-CO_2eq/GJ_e**

While the baseline avoidance cost of 26.7 USD/t-CO_2eq might look favorable compared to CO_2 capture, the algal cultivator system and CO_2 capture are not exactly comparable. There are certain physical (diffusion) and mass transfer limitations that define how much of flue gas CO_2 bubbled into the cultivator broth ends up as biomass. CO_2 must first be dissolved in media (diffusion), which forms bicarbonate (HCO_3^-). Bicarbonate is then absorbed and transported across the algal cell wall (mass transfer) for photosynthesis. The effectiveness of the cultivation broth to uptake and fix the dissolved CO_2 is expressed by the utilization efficiency, which is calculated from mean algal biomass productivity and the flue gas flow rate per volume of media (vvm). For the current microalgal system, the calculated efficiency is 35.6% (Figure SI 10), while the maximum is 46%. Thus, the majority of bubbled CO_2 either remains dissolved in media or collects at the top of the cultivating column to be purged from the reactor. Utilization efficiencies for pond reactors are typically much lower, ranging from 10–30% [37].

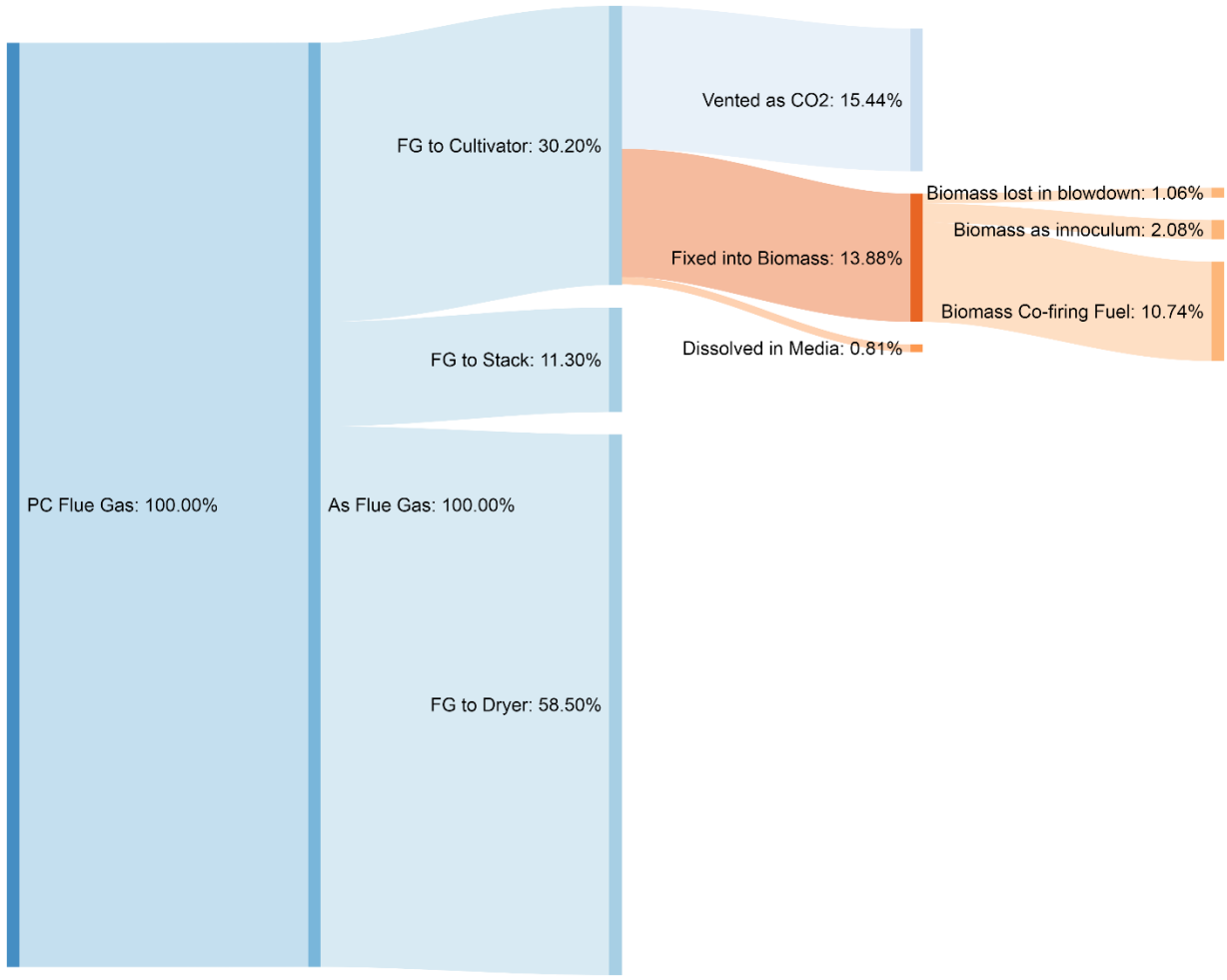

Figure SI 10. Sankey plot of the co-firing plant showing the carbon balance in kt/yr. Less than 36% of the carbon routed to the cultivator ends up in the biomass fuel.

7.5 Sensitivity Analysis

Sensitivity analysis of the cultivation plant with respect to the LCOE, carbon footprint, and GHG avoidance cost are performed. The results are displayed in Figure SI 11. Each metric had different levels of sensitivity with respect to the parameters studied. Biomass LHV and downstream recoveries rank consistently higher than parameters such as flue gas flowrate and cultivation cost. LCOE was most sensitive to the cost of the raw materials, which had a negligible impact on carbon footprint. Note that the sensitivity

chart for the GHG avoidance cost is rather asymmetric, which means that the trade-off cost does not scale proportionally with respect to many of the plant parameters.

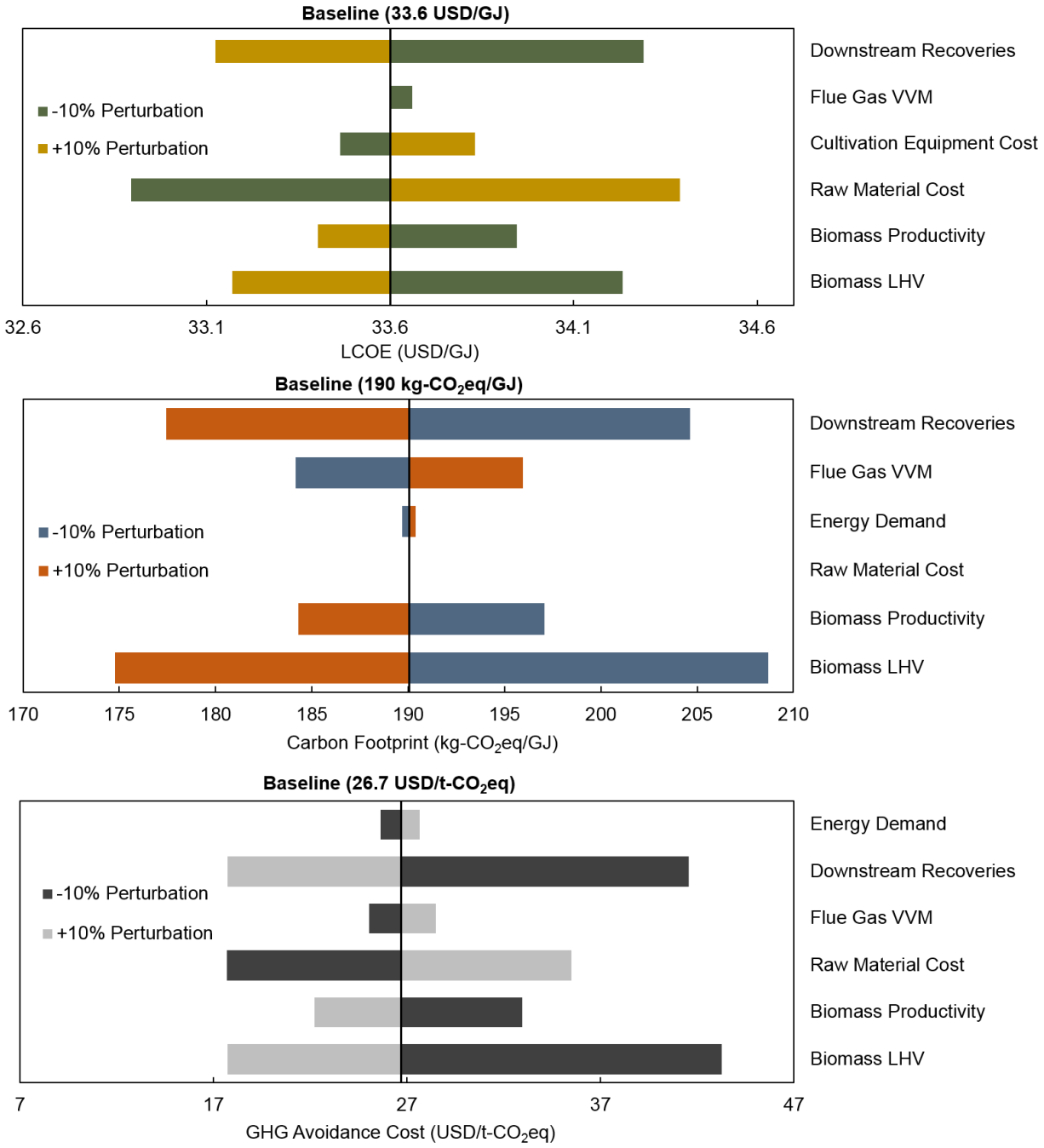

Figure SI 11. Sensitivity analysis of major plant parameters (±10% changes) with respect to LCOE (top), carbon footprint (middle), and GHG avoidance cost (bottom).

Reference

1 G. A. Buchner, K. J. Stepputat, A. W. Zimmermann and R. Schomäcker, Specifying Technology Readiness Levels (TRL) for the Chemical Industry, *Ind. Eng. Chem. Res.*, 2019, acs.iecr.8b05693.

2 E. Rotstein, D. Resasco and G. Stephanopoulos, Studies on the Synthesis of Chemical Reaction Paths - I: Reaction Characteristics in the (G, T) Space and a Primitive Synthesis Procedure, *Chem. Eng. Sci.*, 1982, **37**, 1337–1352.

3 M. Aresta, A. Dibenedetto and E. Quaranta, *Reaction Mechanisms in Carbon Dioxide Conversion*, Springer Berlin Heidelberg, Berlin, Heidelberg, 2016.

4 AACE International, *Cost Estimate Classification System - AACE International Recommended Practice No. 17R-97*, WV, USA, 2019.

5 A. Zimmermann, J. Wunderlich, G. Buchner, L. Müller, K. Armstrong, S. Michailos, A. Marxen, H. Naims, F. Mason, G. Stokes and E. Williams, *Techno-Economic Assessment & Life-Cycle Assessment Guidelines for CO2 Utilization*, 2018.

6 A. Fredenslund, R. L. Jones and J. M. Prausnitz, Group-contribution estimation of activity coefficients in nonideal liquid mixtures, *AIChE J.*, 1975, **21**, 1086–1099.

7 ICIS, ICIS Pricing, https://www.icis.com/about/price-reports/, (accessed 2 September 2018).

8 Zauba, USA Import Data, https://www.zauba.com/USA-imports-exports/Imports, (accessed 6 December 2018).

9 IHS Markit, Chemical Industry Market Intelligence - Market Information, Analysis & Forecasts Reports & Services, https://ihsmarkit.com/industry/chemical.html, (accessed 6 December 2018).

10 E. S. Rubin, J. E. Davison and H. J. Herzog, The cost of CO_2 capture and storage, *Int. J. Greenh. Gas Control*, 2015, **40**, 378–400.

11 M. M. F. Hasan, F. Boukouvala, E. L. First and C. A. Floudas, Nationwide, regional, and statewide CO_2 Capture, Utilization, and Sequestration supply chain network optimization, *Ind. Eng. Chem. Res.*, 2014, **53**, 7489–7506.

12 D. Leeson, N. Mac Dowell, N. Shah, C. Petit and P. S. Fennell, A Techno-economic analysis and systematic review of carbon capture and storage (CCS) applied to the iron and steel, cement, oil refining and pulp and paper industries, as well as other high purity sources, *Int. J. Greenh. Gas Control*, 2017, **61**, 71–84.

13 L. Irlam, *GLOBAL COSTS OF CARBON CAPTURE AND STORAGE - 2017 Update*, 2017.

14 W. Chung, Korea Advanced Institute of Science and Technology, 2019.

15 Eurostat, Database - Eurostat, https://ec.europa.eu/eurostat/data/database, (accessed 4 September 2018).

16 Markets Insider, CO_2 European Emission Allowances, https://markets.businessinsider.com/commodities/co2-emissionsrechte, (accessed 20 July 2018).

17 Grand View Research, Grand View Research homepage, https://www.grandviewresearch.com/, (accessed 9 October 2018).

18 Statista, Statista– The portal for statistics, https://www.statista.com/, (accessed 9 October 2018).

19 Eurostat, Prodcom - Statistics by Product, https://ec.europa.eu/eurostat/web/prodcom, (accessed 6 December 2018).

20 R. Turton, R. C. Bailie and W. Whiting, *Analysis, synthesis, and design of chemical processes*, Prentice Hall, 2012.

21 M. S. Peters, K. D. Timmerhaus and R. E. West, *Plant design and economics for chemical engineers.*, McGraw-Hill, 2003.

22 Kenneth M. Guthrie, Data and techniques for preliminary capital cost estimating, *Chem. Eng.*, 1969, **24**, 114–142.

23 M. M. El-Halwagi, *Sustainable Design Through Process Integration : Fundamentals and Applications to Industrial Pollution Prevention, Resource Conservation, and Profitability Enhancement.*, Elsevier Science, 2011.

24 S. M. Saba, M. Müller, M. Robinius and D. Stolten, The investment costs of electrolysis – A comparison of cost studies from the past 30 years, *Int. J. Hydrogen Energy*, 2018, **43**, 1209–1223.

25 ecoinvent, ecoinvent Database Version 3.01, https://ecoquery.ecoinvent.org/Search/Index, (accessed 4 November 2018).

26 J. Marriott and J. Littlefield, Life Cycle Assessment of Natural Gas Extraction, Delivery and Electricity Production, *Natl. Energy Technol. Lab.*, 2012, 1–23.

27 IINAS, GEMIS - Global Emissions Model for integrated Systems, http://iinas.org/gemis.html, (accessed 9 October 2018).

28 thinkstep AG, GaBi 8.7.18. Software-System and Database for Life Cycle Engineering, http://www.gabi-software.com/international/software/, (accessed 16 October 2018).

29 S. Schlömer, T. Bruckner, L. Fulton, E. Hertwich, A. McKinnon, D. Perczyk, J. Roy, R. Schaeffer, R. Sims, P. Smith and R. Wiser, in *Climate Change 2014: Mitigation of Climate Change. Contribution of Working Group III to the Fifth Assessment Report of the Intergovernmental Panel on Climate Change*, eds. O. Edenhofer, R. Pichs-Madruga, Y. Sokona, E. Farahani, S. Kadner, K. Seyboth, A. Adler, I. Baum, S. Brunner, P. Eickemeier, B. Kriemann, J. Savolainen, S. Schlömer, C. von Stechow, T. Zwickel and J. C. Minx, Cambridge University Press, Cambridge, United Kingdom and New York, NY, USA., 2014.

30 Winnipeg, *Emission factors in kg CO_2-equivalent per unit*, 2012.

31 US EPA, *Emission Factors for Greenhouse Gas Inventories*, 2014.

32 N. von der Assen, L. J. Müller, A. Steingrube, P. Voll and A. Bardow, Selecting CO_2 Sources for CO_2 Utilization by Environmental-Merit-Order Curves, *Environ. Sci. Technol.*, 2016, **50**, 1093–1101.

33 M. E. Boot-Handford, J. C. Abanades, E. J. Anthony, M. J. Blunt, S. Brandani, N. Mac Dowell, J. R. Fernández, M.-C. Ferrari, R. Gross, J. P. Hallett, R. S. Haszeldine, P. Heptonstall, A. Lyngfelt, Z. Makuch, E. Mangano, R. T. J. Porter, M. Pourkashanian, G. T. Rochelle, N. Shah, J. G. Yao and P. S. Fennell, Carbon capture and storage update, *Energy Environ. Sci.*, 2014, **7**, 130–189.

34 S. Ga, H. Jang and J. H. Lee, New performance indicators for adsorbent evaluation derived from a reduced order model of an idealized PSA process for CO_2 capture, *Comput. Chem. Eng.*, 2017, **102**, 188–212.

35 NIST, NIST Chemistry WebBook, https://webbook.nist.gov/chemistry/, (accessed 2 September 2018).

36 O. K. Dalrymple, T. Halfhide, I. Udom, B. Gilles, J. Wolan, Q. Zhang and S. Ergas, Wastewater use in algae production for generation of renewable resources: a review and preliminary results, *Aquat. Biosyst.*, 2013, **9**, 2.

37 L. Stryer, *Biochemistry*, W.H. Freeman and Company, 2nd edn., 1981.

38 C. A. Jaksland, R. Gani and K. M. Lien, Separation process design and synthesis based on thermodynamic insights, *Chem. Eng. Sci.*, 1995, **50**, 511–530.

39 A. J. Bard and L. R. Faulkner, *Electrochemical methods : fundamentals and applications*, Wiley, 2001.

40 S. A. Amelkin, A. M. Tsirlin, J. M. Burzler, S. Schubert and K. H. Hoffmann, Minimal work for separation processes of binary mixtures, *Open Syst. Inf. Dyn.*, 2003, **10**, 335–349.

41 M. R. Droop, Vitamin B 12 and Marine Ecology. IV. The Kinetics of Uptake, Growth and Inhibition in Monochrysis Lutheri, *J. Mar. Biol. Assoc. United Kingdom*, 1968, **48**, 689–733.

42 Y. Zhang, J. Cruz, S. Zhang, H. H. Lou and T. J. Benson, Process simulation and optimization of methanol production coupled to tri-reforming process, *Int. J. Hydrogen Energy*, 2013, **38**, 13617–13630.

43 I. C. Kemp, *Pinch Analysis and Process Integration*, Elsevier, 2007.

44 B. Linnhoff and E. Hindmarsh, The pinch design method for heat exchanger networks, *Chem. Eng. Sci.*, 1983, **38**, 745–763.

45 AVT, EE-Toolbox, http://www.avt.rwth-aachen.de/cms/AVT/Forschung/Software/~iptv/Shortcut-Toolbox/?lidx=1, (accessed 16 October 2018).

46 J. Bausa, R. v. Watzdorf and W. Marquardt, Shortcut methods for nonideal multicomponent distillation: I. Simple columns, *AIChE J.*, 1998, **44**, 2181–2198.

47 S. Kossack, K. Kraemer, R. Gani and W. Marquardt, A systematic synthesis framework for extractive distillation processes, *Chem. Eng. Res. Des.*, 2008, **86**, 781–792.

48 K. Kraemer, A. Harwardt, M. Skiborowski, S. Mitra and W. Marquardt, Shortcut-based design of multicomponent heteroazeotropic distillation, *Chem. Eng. Res. Des.*, 2011, **89**, 1168–1189.

49 K. Kraemer, S. Kossack and W. Marquardt, Efficient Optimization-Based Design of Distillation Processes for Homogeneous Azeotropic Mixtures, *Ind. Eng. Chem. Res.*, 2009, **48**, 6749–6764.

50 C. Redepenning and W. Marquardt, Pinch-based shortcut method for the conceptual design of adiabatic absorption columns, *AIChE J.*, 2017, **63**, 1213–1225.

51 R. von Watzdorf, J. Bausa and W. Marquardt, Shortcut methods for nonideal multicomponent distillation: 2. Complex columns, *AIChE J.*, 1999, **45**, 1615–1628.

52 R. Y. Urdaneta, J. Bausa, S. Brüggemann and W. Marquardt, Analysis and Conceptual Design of Ternary Heterogeneous Azeotropic Distillation Processes, *Ind. Eng. Chem. Res.*, 2002, **41**, 3849–3866.

53 A. Harwardt, S. Kossack and W. Marquardt, in *Computer Aided Chemical Engineering*, Elsevier, 2008, vol. 25, pp. 91–96.

54 W. Schakel, C. Fernández-Dacosta, M. van der Spek and A. Ramírez, New indicator for comparing the energy performance of CO_2 utilization concepts, *J. CO2 Util.*, 2017, **22**, 278–288.

55 T. Blumberg, T. Morosuk and G. Tsatsaronis, Exergy-based evaluation of methanol production from natural gas with CO_2 utilization, *Energy*, 2017, **141**, 2528–2539.

56 K. Roh, A. S. Al-Hunaidy, H. Imran and J. H. Lee, Optimization-based identification of CO_2 capture and utilization processing paths for life cycle greenhouse gas reduction and economic benefits, *AIChE J.*, 2019, **65**, e16580.

57 N. von der Assen, P. Voll, M. Peters and A. Bardow, Life cycle assessment of CO_2 capture and utilization: a tutorial review., *Chem. Soc. Rev.*, 2014, **43**, 7982–94.

58 K. Roh, H. Lim, W. Chung, J. Oh, H. Yoo, A. S. Al-Hunaidy, H. Imran and J. H. Lee, Sustainability analysis of CO_2 capture and utilization processes using a computer-aided tool, *J. CO2 Util.*, 2018, **26**, 60–69.

59 K. Roh, J. H. Lee and R. Gani, A methodological framework for the development of feasible CO_2 conversion processes, *Int. J. Greenh. Gas Control*, 2016, **47**, 250–265.

60 G. A. Olah, A. Goeppert and G. K. S. Prakash, *Beyond Oil and Gas: The Methanol Economy: Second Edition*, 2009.

61 S. Deutz, D. Bongartz, B. Heuser, A. Kätelhön, L. Schulze Langenhorst, A. Omari, M. Walters, J. Klankermayer, W. Leitner, A. Mitsos, S. Pischinger and A. Bardow, Cleaner production of cleaner fuels: wind-to-wheel – environmental assessment of CO_2-based oxymethylene ether as a drop-in fuel, *Energy Environ. Sci.*, 2018, **11**, 331–343.

62 J. Jung, N. von der Assen and A. Bardow, Comparative LCA of multi-product processes with non-common products: a systematic approach applied to chlorine electrolysis technologies, *Int. J. Life Cycle Assess.*, 2013, **18**, 828–839.

63 G. A. Buchner, A. W. Zimmermann, A. E. Hohgräve and R. Schomäcker, Techno-economic Assessment Framework for the Chemical Industry—Based on Technology Readiness Levels, *Ind. Eng. Chem. Res.*, 2018, **57**, 8502–8517.

64 L. T. L. T. Biegler, I. E. I. E. Grossmann and A. W. A. W. Westerberg, *Systematic Methods of Chemical Process Design*, Prentice Hall, New Jersey, 1st edn., 1997.

65 M. Tsagkari, J.-L. Couturier, A. Kokossis and J.-L. Dubois, Early-Stage Capital Cost Estimation of Biorefinery Processes: A Comparative Study of Heuristic Techniques, *ChemSusChem*, 2016, **9**, 2284–2297.

66 J. M. Spurgeon and B. Kumar, A comparative technoeconomic analysis of pathways for commercial electrochemical CO reduction to liquid products, *Energy Environ. Sci.*, 2018, **11**, 1536–1551.

67 Reaxys, Reaxys Support Center, https://service.elsevier.com/app/answers/detail/a_id/13722/supporthub/reaxys/, (accessed 16 October 2018).

68 CAS, SciFinder, https://www.cas.org/products/scifinder, (accessed 16 October 2018).

69 AIChE, DIPPR, https://www.aiche.org/dippr, (accessed 16 October 2018).

70 DDBST GmbH, DDBST, http://www.ddbst.de/, (accessed 16 October 2018).

71 DECHEMA, Detherm, https://dechema.de/dechema_eV/en/detherm-p-24.html, (accessed 16 October 2018).

72 Aspen Technology, Aspen Plus, https://www.aspentech.com/products/engineering/aspen-plus, (accessed 7 August 2018).

73 Aspen Technology, Aspen HYSYS, https://www.aspentech.com/en/products/engineering/aspen-hysys, (accessed 16 October 2018).

74 Schneider Electric Software, PRO/II Comprehensive Process Simulation, http://iom.invensys.com/AP/Pages/SimSci_ProcessEngSuite_PROII.aspx, (accessed 8 August 2018).

75 Chemstations, CHEMCAD, https://www.chemstations.com/CHEMCAD/, (accessed 16 October 2018).

76 Intelligen, SuperPro Designer, http://www.intelligen.com/superpro_overview.html, (accessed 16 October 2018).

77 A. K. Tula, D. K. Babi, J. Bottlaender, M. R. Eden and R. Gani, A computer-aided software-tool for sustainable process synthesis-intensification, *Comput. Chem. Eng.*, 2017, **105**, 74–95.

78 PSE for SPEED, ProCAFD – Computer Aided Flowsheet Design, http://www.pseforspeed.com/procafd/, (accessed 16 October 2018).

79 J. Steimel, M. Harrmann, G. Schembecker and S. Engell, Model-based conceptual design and optimization tool support for the early stage development of chemical processes under uncertainty, *Comput. Chem. Eng.*, 2013, **59**, 63–73.

80 J. Marrero and R. Gani, Group-contribution based estimation of pure component properties, *Fluid Phase Equilib.*, 2001, **183**–**184**, 183–208.

81 PSE for SPEED, ProPred, http://www.pseforspeed.com/icas/propred/, (accessed 16 October 2018).

82 A. Klamt and G. Schüürmann, COSMO: a new approach to dielectric screening in solvents with explicit expressions for the screening energy and its gradient, *J. Chem. Soc., Perkin Trans. 2*, 1993, 799–805.

83 A. Klamt, Conductor-like Screening Model for Real Solvents: A New Approach to the Quantitative Calculation of Solvation Phenomena, *J. Phys. Chem.*, 1995, **99**, 2224–2235.

84 COSMOlogic, COSMOtherm: Predicting Solutions since 1999, http://www.cosmologic.de/products/cosmotherm.html, (accessed 16 October 2018).

85 PRé Sustainability, SimaPro, https://simapro.com/, (accessed 16 October 2018).

86 T. Rattanatum, R. Frauzem, P. Malakul and R. Gani, in *Computer Aided Chemical Engineering*, Elsevier, 2018, vol. 43, pp. 13–18.

87 Y. Chavewanmas, P. Malakul and R. Gani, in *Computer Aided Chemical Engineering*, Elsevier, 2017, vol. 40, pp. 2305–2310.

88 PSE for SPEED, LCSoft, http://www.pseforspeed.com/icas/lcsoft/, (accessed 16 October 2018).

89 Aspen Technology, Aspen Process Economic Analyzer, https://www.aspentech.com/en/products/pages/aspen-process-economic-analyzer, (accessed 16 October 2018).

90 PSE for SPEED, ECON, http://www.pseforspeed.com/icas/econ/, (accessed 16 October 2018).

91 ERC Association, ERC Publishes Early-Stage Technoeconomic Evaluation (ESTEA) Tool, http://erc-assoc.org/achievements/erc-publishes-early-stage-technoeconomic-evaluation-estea-tool, (accessed 15 June 2019).

92 LENSE, Manual and tutorial of ArKa-TAC3, http://lense.kaist.ac.kr/bbs/board.php?bo_table=sub05_3&wr_id=7, (accessed 16 October 2018).

93 J. S. Lee, Development of a Computer-Aided Tool for high-throughput Analysis and Evaluation of low-TRL Microalgal Systems for Process Synthesis, Korea Advanced Institute of Science and Technology, Master thesis, 2019.

94 Palisade, @RISK: Risk Analysis using Monte Carlo Simulation in Excel and Project, http://www.palisade.com/risk/default.asp, (accessed 16 October 2018).

95 GAMS Software GmbH, GAMS, https://www.gams.com/, (accessed 16 October 2018).

96 FICO, FICO® Xpress Optimization, https://www.fico.com/en/products/fico-xpress-optimization, (accessed 16 October 2018).

97 W. E. Hart, C. Laird, J.-P. Watson and D. L. Woodruff, *Pyomo – Optimization Modeling in Python*, Springer US, Boston, MA, Second., 2012, vol. 67.

98 W. E. Hart, J.-P. Watson and D. L. Woodruff, Pyomo: modeling and solving mathematical programs in Python, *Math. Program. Comput.*, 2011, **3**, 219–260.

99 A. Voll and W. Marquardt, Reaction network flux analysis: Optimization-based evaluation of reaction pathways for biorenewables processing, *AIChE J.*, 2012, **58**, 1788–1801.

100 K. Ulonska, M. Skiborowski, A. Mitsos and J. Viell, Early-stage evaluation of biorefinery processing pathways using process network flux analysis, *AIChE J.*, 2016, **62**, 3096–3108.

101 S. Roman-White, S. Rai, J. Littlefield, G. Cooney and T. J. Skone, *Life cycle greenhouse gas perspective on exporting liquefied natural gas from the united states: 2019 update*, Pittsburgh, 2019.

102 S. K. Dube, P. Vasudevan and B. L. Khandelwal, Oxalic acid manufacture, *J. Chem. Technol. Biotechnol.*, 2007, **32**, 909–919.

103 A. Nette, P. Wolf, O. Schlüter and A. Meyer-Aurich, A Comparison of Carbon Footprint and Production Cost of Different Pasta Products Based on Whole Egg and Pea Flour, *Foods*, 2016, **5**, 17.

104 J. Kim, C. a. Henao, T. a. Johnson, D. E. Dedrick, J. E. Miller, E. B. Stechel and C. T. Maravelias, Methanol production from CO_2 using solar-thermal energy: process development and techno-economic analysis, *Energy Environ. Sci.*, 2011, **4**, 3122.

105 S. Licht, H. Wu, C. Hettige, B. Wang, J. Asercion, J. Lau and J. Stuart, STEP cement: Solar Thermal Electrochemical Production of CaO without CO_2 emission, *Chem. Commun.*, 2012, **48**, 6019.

106 KPRC, Price data, http://www.kprc.or.kr/main.do?menuID=100000, (accessed 12 October 2017).

107 Korea Gas Cooperation, Natural Gas Price for Power Generation, http://www.kogas.or.kr/portal/contents.do?key=2017, (accessed 28 March 2020).

108 S&P Global Platts, Platts Global Ethylene Price Index, https://www.spglobal.com/platts/en/our-methodology/price-assessments/petrochemicals/pgpi-ethylene, (accessed 28 November 2018).

109 U.S. GRAINS COUNCIL, Ethanol Market and Pricing Data - February 20, 2018, https://grains.org/ethanol_report/ethanol-market-and-pricing-data-february-20-2018/, (accessed 28 November 2018).

110 Alibaba, Oxalic Acid Price, https://www.alibaba.com/showroom/oxalic-acid-price.html, (accessed 28 November 2018).

111 A. Ebrahimi, M. Meratizaman, H. Akbarpour Reyhani, O. Pourali and M. Amidpour, Energetic, exergetic and economic assessment of oxygen production from two columns cryogenic air separation unit, *Energy*, 2015, **90**, 1298–1316.

112 KASIO, *Levelized cost of electricity: Overseas case study and implication analysis*, Naju, South Korea, 2018.

113 Orbis Research, Global Carbon Monoxide Market 2017 Forecast to 2022, https://www.orbisresearch.com/reports/index/global-north-america-europe-and-asia-pacific-south-america-middle-east-and-africa-carbon-monoxide-market-2017-forecast-to-2022, (accessed 2 February 2020).

114 J. Hietala, A. Vuori, P. Johnsson, I. Pollari, W. Reutemann and H. Kieczka, in *Ullmann's Encyclopedia of Industrial Chemistry*, Wiley-VCH Verlag GmbH & Co. KGaA, Weinheim, Germany, 2016, vol. 1, pp. 1–22.

115 Methanol Institute, METHANOL PRICE AND SUPPLY/DEMAND, https://www.methanol.org/methanol-price-supply-demand/, (accessed 20 February 2020).

116 M. Jouny, W. Luc and F. Jiao, General Techno-Economic Analysis of CO2 Electrolysis Systems, *Ind. Eng. Chem. Res.*, 2018, **57**, 2165–2177.

117 S. Lewandowski, Ethylene - Global, https://cdn.ihs.com/www/pdf/Steve-Lewandowski-Big-Changes-Ahead-for-Ethylene-Implications-for-Asia.pdf, (accessed 20 February 2020).

118 Transparency Market Research, GLOBAL ETHANOL MARKET: ADVANCEMENT IN PRODUCTION TECHNOLOGIES TO BOOST MARKET, NOTES TMR, https://www.transparencymarketresearch.com/pressrelease/ethanol-market.htm, (accessed 20 February 2020).

119 W. Riemenschneider and M. Tanifuji, in *Ullmann's Encyclopedia of Industrial Chemistry*, Wiley-VCH Verlag GmbH & Co. KGaA, Weinheim, Germany, 2011, pp. 543–600.

120 J. Klabunde, C. Bischoff and A. J. Papa, in *Ullmann's Encyclopedia of Industrial Chemistry*, Wiley-VCH Verlag GmbH & Co. KGaA, Weinheim, Germany, 2018, pp. 1–14.

121 Pharkya P, Burgard AP, Osterhout RE, Burk MJ, Sun J. Microorganisms and methods for the co-production of isopropanol with primary alcohols, diols and acids. WO 2011/031897 Al, 2011.

122 G. Wernet, C. Bauer, B. Steubing, J. Reinhard, E. Moreno-Ruiz and B. Weidema, The ecoinvent database version 3 (part I): overview and methodology, *Int. J. Life Cycle Assess.*, 2016, **21**, 1218–1230.

123 S. Fazio, V. Castellani, S. Sala, E. M. Schau, M. Secchi and L. Zampori, *Supporting information to the characterisation factors of recommended EF Life Cycle Impact Assessment methods: EUR 28888 EN, European Commission, Ispra, 2, JRC109369*, Publications Office of the European

Union, 2018.

124 J.-B. Vennekoetter, R. Sengpiel and M. Wessling, Beyond the catalyst: How electrode and reactor design determine the product spectrum during electrochemical CO_2 reduction, *Chem. Eng. J.*, 2019, **364**, 89–101.

125 F. P. García de Arquer, C. Dinh, A. Ozden, J. Wicks, C. McCallum, A. R. Kirmani, D. Nam, C. Gabardo, A. Seifitokaldani, X. Wang, Y. C. Li, F. Li, J. Edwards, L. J. Richter, S. J. Thorpe, D. Sinton and E. H. Sargent, CO_2 electrolysis to multicarbon products at activities greater than 1 A cm−2, *Science (80-.).*, 2020, **367**, 661–666.

126 A. Engelbrecht, C. Uhlig, O. Stark, M. Hämmerle, G. Schmid, E. Magori, K. Wiesner-Fleischer, M. Fleischer and R. Moos, On the Electrochemical CO_2 Reduction at Copper Sheet Electrodes with Enhanced Long-Term Stability by Pulsed Electrolysis, *J. Electrochem. Soc.*, 2018, **165**, J3059–J3068.

127 C. Reller, R. Krause, E. Volkova, B. Schmid, S. Neubauer, A. Rucki, M. Schuster and G. Schmid, Selective Electroreduction of CO_2 toward Ethylene on Nano Dendritic Copper Catalysts at High Current Density, *Adv. Energy Mater.*, 2017, **7**, 1602114.

128 O. S. Bushuyev, P. De Luna, C. T. Dinh, L. Tao, G. Saur, J. van de Lagemaat, S. O. Kelley and E. H. Sargent, What Should We Make with CO_2 and How Can We Make It?, *Joule*, 2018, **2**, 825–832.

129 I. Amghizar, L. A. Vandewalle, K. M. Van Geem and G. B. Marin, New Trends in Olefin Production, *Engineering*, 2017, **3**, 171–178.

130 H. Yano, T. Tanaka, M. Nakayama and K. Ogura, Selective electrochemical reduction of CO_2 to ethylene at a three-phase interface on copper(I) halide-confined Cu-mesh electrodes in acidic solutions of potassium halides, *J. Electroanal. Chem.*, 2004, **565**, 287–293.

131 M. Scholz, B. Frank, F. Stockmeier, S. Falß and M. Wessling, Techno-economic Analysis of Hybrid Processes for Biogas Upgrading, *Ind. Eng. Chem. Res.*, 2013, **52**, 16929–16938.

132 Korea Electric Power Cooperation, Electric Rates Table in South Korea, http://cyber.kepco.co.kr/ckepco/front/jsp/CY/E/E/CYEEHP00201.jsp, (accessed 28 November 2018).

133 F. Ausfelder, A. Seitz and S. von Roon, *Flexibilitätsoptionen in der Grundstoffindustrie : Methodik, Potenziale, Hemmnisse*, Frankfurt am Main, 2018.

134 L. Zhao, R. Menzer, E. Riensche, L. Blum and D. Stolten, Concepts and investment cost analyses of multi-stage membrane systems used in post-combustion processes, *Energy Procedia*, 2009, **1**, 269–278.

135 H. Lin and B. D. Freeman, Gas Permeation and Diffusion in Cross-Linked Poly(ethylene glycol diacrylate), *Macromolecules*, 2006, **39**, 3568–3580.

136 M. Scholz, T. Harlacher, T. Melin and M. Wessling, Modeling Gas Permeation by Linking Nonideal Effects, *Ind. Eng. Chem. Res.*, 2013, **52**, 1079–1088.

137 Strobridge TR, *Cryogenic refrigerators----An updated survey: National Bureau of Standards Technical Note 655 (Supt. Documents, U.S. Govt. Printing Off.)*, 1974.

138 H. J. M. ter Brake and G. F. M. Wiegerinck, Low-power cryocooler survey, *Cryogenics (Guildf).*, 2002, **42**, 705–718.

139 L. J. Müller, A. Kätelhön, M. Bachmann, A. Zimmermann, A. Sternberg and A. Bardow, A Guideline for Life Cycle Assessment of Carbon Capture and Utilization, *Front. Energy Res.*, 2020, **8**, 1.

140 International Organization for Standardization, ISO 14040 - Environmental management - Life cycle assessment - Principles and framework, 2006.

141 International Organization for Standardization, ISO 14044: Environmental Management: Life Cycle Assessment: Requirements and Guidelines, 2006.

142 N. von der Assen, L. J. Müller, A. Steingrube, P. Voll and A. Bardow, Selecting CO_2 Sources for CO_2 Utilization by Environmental-Merit-Order Curves, *Environ. Sci. Technol.*, 2016, **50**, 1093–1101.

143 A. Sternberg and A. Bardow, Life cycle assessment of power-to-gas: Syngas vs Methane, *ACS Sustain. Chem. Eng.*, 2016, **4**, 4156–4165.

144 IPCC, *Climate Change 2013: The Physical Science Basis. Contribution of Working Group I to the Fifth Assessment Report of the Intergovernmental Panel on Climate ChangeThe physical science basis: [Stocker, T.F., D. Qin, G.-K. Plattner, M. Tignor, S.K. Allen, J. B*, Cambridge University Press, Cambridge, United Kingdom and New York, NY, USA, 2013.

145 T. Burdyny and W. A. Smith, CO_2 reduction on gas-diffusion electrodes and why catalytic performance must be assessed at commercially-relevant conditions, *Energy Environ. Sci.*, 2019, **12**, 1442–1453.

146 F. Pontzen, W. Liebner, V. Gronemann, M. Rothaemel and B. Ahlers, CO_2-based methanol and DME - Efficient technologies for industrial scale production, *Catal. Today*, 2011, **171**, 242–250.

147 M. Bertau, H. Offermanns, L. Plass, F. Schmidt and H.-J. Wernicke, *Methanol: The Basic Chemical and Energy Feedstock of the Future*, Springer Berlin Heidelberg, Berlin, Heidelberg, 2014.

148 Z. Fan, H. Guo, K. Fang and Y. Sun, Efficient V_2O_5/TiO_2 composite catalysts for dimethoxymethane synthesis from methanol selective oxidation, *RSC Adv.*, 2015, **5**, 24795–24802.

149 E. Zhan, Y. Li, J. Liu, X. Huang and W. Shen, A VOx/meso-TiO_2 catalyst for methanol oxidation to dimethoxymethane, *Catal. Commun.*, 2009, **10**, 2051–2055.

150 Q. Sun, J. Liu, J. Cai, Y. Fu and J. Shen, Effect of silica on the selective oxidation of methanol to dimethoxymethane over vanadia–titania catalysts, *Catal. Commun.*, 2009, **11**, 47–50.

151 A. Omari, B. Heuser and S. Pischinger, Potential of oxymethylenether-diesel blends for ultra-low emission engines, *Fuel*, 2017, **209**, 232–237.

152 K. Bareiß, C. de la Rua, M. Möckl and T. Hamacher, Life cycle assessment of hydrogen from proton exchange membrane water electrolysis in future energy systems, *Appl. Energy*, 2019, **237**, 862–872.

153 T. Grube, L. Doré, A. Hoffrichter, L. E. Hombach, S. Raths, M. Robinius, M. Nobis, S. Schiebahn, V. Tietze, A. Schnettler, G. Walther and D. Stolten, An option for stranded renewables: electrolytic-hydrogen in future energy systems, *Sustain. Energy Fuels*, 2018, **2**, 1500–1515.

154 H. Renon and J. M. Prausnitz, Local compositions in thermodynamic excess functions for liquid mixtures, *AIChE J.*, 1968, **14**, 135–144.

155 J.-O. Weidert, J. Burger, M. Renner, S. Blagov and H. Hasse, Development of an Integrated

Reaction–Distillation Process for the Production of Methylal, *Ind. Eng. Chem. Res.*, 2017, **56**, 575–582.

156 AGEB, AG Energiebilanzen e.V. | Berichte, https://ag-energiebilanzen.de/index.php?article_id=20&archiv=13&year=2018, (accessed 7 January 2019).

157 Chemical Engineering, CHEMICAL ENGINEERING PLANT COST INDEX: 2018 ANNUAL VALUE, https://www.chemengonline.com/2019-cepci-updates-january-prelim-and-december-2018-final/, (accessed 25 April 2020).

158 H. Althaus, M. Chudacoff, R. Hischier, N. Jungbluth, M. Osses, A. Primas and S. Hellweg, Life cycle inventories of chemicals. ecoinvent report No.8, v2.0., *Final Rep. ecoinvent data …*, 2007, 1–957.

159 M. Reuter, O. Oyj, C. Hudson, A. van Schaik, K. Heiskanen, C. Meskers and C. Hagelüken, 2013.

160 IEA and International Energy Agency, *Energy Technology Perspectives 2017*, OECD, 2017.

161 OECD/IEA, *Energy Technology Perspectives 2017 - Catalysing Energy Technology Transformations*, Paris, France, 2017.

162 A. D. Kroumov, A. N. Módenes, D. E. G. Trigueros, F. R. Espinoza-Quiñones, C. E. Borba, F. B. Scheufele and C. L. Hinterholz, A systems approach for CO_2 fixation from flue gas by microalgae—Theory review, *Process Biochem.*, 2016, **51**, 1817–1832.

163 C. Ji, J. Wang, R. Li and T. Liu, Modeling of carbon dioxide mass transfer behavior in attached cultivation photobioreactor using the analysis of the pH profiles, *Bioprocess Biosyst. Eng.*, 2017, **40**, 1079–1090.

164 R. W. Babcock, J. Malda and J. C. Radway, Hydrodynamics and mass transfer in a tubular airlift photobioreactor, *J. Appl. Phycol.*, 2002, **14**, 169–184.

165 R. J. Ellis, Tackling unintelligent design, *Nature*, 2010, **463**, 164–165.

166 S. Li, S. Luo and R. Guo, Efficiency of CO_2 fixation by microalgae in a closed raceway pond, *Bioresour. Technol.*, 2013, **136**, 267–272.

167 A. K. Lee, D. M. Lewis and P. J. Ashman, Harvesting of marine microalgae by electroflocculation: The energetics, plant design, and economics, *Appl. Energy*, 2013, **108**, 45–53.

168 H. Li, Q. Chen, X. Zhang, K. N. Finney, V. N. Sharifi and J. Swithenbank, Evaluation of a biomass drying process using waste heat from process industries: A case study, *Appl. Therm. Eng.*, 2012, **35**, 71–80.

169 Q. Gong, Y. Feng, L. Kang, M. Luo and J. Yang, Effects of Light and pH on Cell Density of Chlorella Vulgaris, *Energy Procedia*, 2014, **61**, 2012–2015.

170 A. Giostri, M. Binotti and E. Macchi, Microalgae cofiring in coal power plants: Innovative system layout and energy analysis, *Renew. Energy*, 2016, **95**, 449–464.

171 R. R. Narala, S. Garg, K. K. Sharma, S. R. Thomas-Hall, M. Deme, Y. Li and P. M. Schenk, Comparison of Microalgae Cultivation in Photobioreactor, Open Raceway Pond, and a Two-Stage Hybrid System, *Front. Energy Res.*, , DOI:10.3389/fenrg.2016.00029.

172 S. Tebbani, F. Lopes, R. Filali, D. Dumur and D. Pareau, *CO_2 Biofixation by Microalgae*, John Wiley & Sons, Inc., Hoboken, NJ, USA, 2014.

173 E. Lee, M. Jalalizadeh and Q. Zhang, Growth kinetic models for microalgae cultivation: A review, *Algal Res.*, 2015, **12**, 497–512.

174 A. Guldhe, R. Misra, P. Singh, I. Rawat and F. Bux, An innovative electrochemical process to alleviate the challenges for harvesting of small size microalgae by using non-sacrificial carbon electrodes, *Algal Res.*, 2016, **19**, 292–298.

175 R. Misra, A. Guldhe, P. Singh, I. Rawat and F. Bux, Electrochemical harvesting process for microalgae by using nonsacrificial carbon electrode: A sustainable approach for biodiesel production, *Chem. Eng. J.*, 2014, **255**, 327–333.

176 A. Sandip, V. H. Smith and T. N. Faddis, An experimental investigation of microalgal dewatering efficiency of belt filter system, *Energy Reports*, 2015, **1**, 169–174.

177 E. H. Dunlop and A. K. Coaldrake, in *ABO Algal Biomass Summit*, San Diego, CA, 2014.

178 G. Markou, D. Vandamme and K. Muylaert, Microalgal and cyanobacterial cultivation: The supply of nutrients, *Water Res.*, 2014, **65**, 186–202.

179 H. P. Loh, J. Lyons and C. White, *Process Equipment Cost Estimation, Final Report*, Morgantown, WV, 2002.

180 M. R. Tredici, L. Rodolfi, N. Biondi, N. Bassi and G. Sampietro, Techno-economic analysis of microalgal biomass production in a 1-ha Green Wall Panel (GWP®) plant, *Algal Res.*, 2016, **19**, 253–263.

181 U.S. EIA, *Capital Cost Estimates for Utility Scale Electricity Generating Plants*, Washington, DC 20585, 2016.